Atmos. Chem. Phys. Discuss., https://doi.org/10.5194/acp-2017-731
Manuscript under review for journal Atmos. Chem. Phys.
Discussion started: 5 September 2017

Atmospheric Chemistry and Physics Discussions

Air Quality and Climate Change, Topic 3 of the Model Inter-Comparison Study for Asia Phase III (MICS-Asia III), Part I: overview and model evaluation

Meng Gao[1,2], Zhiwei Han[3,4], Zirui Liu[5], Meng Li[6, 13], Jinyuan Xin[5], Zhining Tao[7,8], Jiawei Li[4], Jeong-Eon Kang[9], Kan Huang[10], Xinyi Dong[10], Bingliang Zhuang[11], Shu Li[11], Baozhu Ge[5], Qizhong Wu[12], Yafang Cheng[13], Yuesi Wang[5], Hyo-Jung Lee[9], Cheol-Hee Kim[9], Joshua S. Fu[10], Tijian Wang[11], Mian Chin[8], Jung-Hun Woo[14], Qiang Zhang[6], Zifa Wang[4,5], Gregory R. Carmichael[1]

1 Center for Global and Regional Environmental Research, University of Iowa, Iowa City, IA, USA

2 John A. Paulson School of Engineering and Applied Sciences, Harvard University, Cambridge, MA, USA

3 Key Laboratory of Regional Climate-Environment for Temperate East Asia, Institute of Atmospheric Physics, Chinese Academy of Sciences, Beijing, China

4 University of Chinese Academy of Sciences, Beijing 100049, China

5 State Key Laboratory of Atmospheric Boundary Layer Physics and Atmospheric Chemistry, Institute of Atmospheric Physics, Chinese Academy of Sciences, Beijing, China

6 Ministry of Education Key Laboratory for Earth System Modeling, Center for Earth System Science, Tsinghua University, Beijing, China

7 Universities Space Research Association, Columbia, MD, USA

8 NASA Goddard Space Flight Center, Greenbelt, MD, USA

9 Department of Atmospheric Sciences, Pusan National University, Busan, South Korea

10 Department of Civil and Environmental Engineering, University of Tennessee, Knoxville, TN, USA

11 School of Atmospheric Sciences, Nanjing University, Nanjing, China

12 College of Global Change and Earth System Science, Beijing Normal University, Beijing, China

13 Multiphase Chemistry Department, Max Planck Institute for Chemistry, Mainz, Germany

14 Department of Advanced Technology Fusion, Konkuk University, Seoul, South Korea

Correspondence to: M. Gao (mgao2@seas.harvard.edu), Z. Han (hzw@mail.iap.ac.cn), and G. R. Carmichael (gcarmich@engineering.uiowa.edu)

Abstract

Topic 3 of the Model Inter-Comparison Study for Asia (MICS-Asia) Phase III examines how online coupled air quality models perform in simulating high aerosol pollution in the North China Plain region during wintertime haze events and evaluates the importance of aerosol radiative and microphysical feedbacks. A comprehensive overview of the MICS-ASIA III Topic 3 study design, including descriptions of participating models and model inputs, the experimental designs, and results of model evaluation, are presented. Two winter months (January 2010 and January 2013) were selected as study periods, when severe haze occurred in North China. Simulations were designed to evaluate radiative and microphysical feedbacks, together and separately, relative to simulations without feedbacks. Six modeling groups from China, Korea and the United States submitted results from seven applications of online coupled chemistry-meteorology models. Results are compared to meteorology and air quality measurements, including the Campaign on Atmospheric Aerosol Research Network of China (CARE-China) network, and the Acid Deposition Monitoring Network in East Asia (EANET). The analysis focuses on model evaluations and aerosol effects on meteorology and air quality, and potentially other interesting topics, such as the impacts of model resolutions on aerosol-radiation-weather

interactions. The model evaluations for January 2010 show that current online-coupled meteorology-chemistry model can generally well reproduced meteorological features and variations of major air pollutants, including aerosol concentrations. The correlation coefficients between multi-model ensemble mean and observed near-surface temperature, water vapor mixing ratio and wind speeds can reach as high as 0.99, 0.99 and 0.98. The correlation coefficients between multi-model ensemble mean and the CARE-China observed near-surface air pollutants range from 0.51 to 0.94 (0.51 for ozone and 0.94 for $PM_{2.5}$). However, large discrepancies exist between simulated aerosol chemical compositions from different models, which is due to different parameterizations of chemical reactions. The coefficient of variation (standard deviation divided by average) can reach above 1.3 for sulfate in Beijing, and above 1.6 for nitrate and organic aerosol in coastal regions, indicating these compositions are less consistent from different models. During clean periods, simulated Aerosol Optical Depths (AOD) from different models are consistent, but peak values differ during severe haze event, which can be explained by the differences in simulated inorganic aerosol concentrations and the hygroscopic growth efficiency (affected by varied RH). These results provide some brief senses of how current online-coupled meteorology-chemistry models reproduce severe haze events, and some directions for future model improvements.

1 Introduction

Air pollution in Asia, particularly in China and India, has been an increasing important research topic, and has attracted enormous media coverage since about 60% of the world population live and are exposed to extremely unhealthy air in this region. It is estimated that outdoor air

pollution brings about 3.3 million premature deaths per year worldwide but primarily in Asia (Lelieveld et al., 2015). In addition, the impacts of regional and intercontinental transport of Asian pollutants on air quality and climate change have been frequently reported (Akimoto, 2003; Menon et al., 2002, Ramanathan and Carmichael, 2008). Chemical transport models have been developed and applied to study various air pollution issues in Asia. For example, an Eulerian regional scale acid deposition and photochemical oxidant model was developed in the United States (Carmichael and Peters, 1984; Carmichael et al., 1986; Carmichael et al., 1991) and applied to study long-range transport of sulfur oxides (SO_x), dust and ozone production in East Asia (Carmichael et al., 1998; Xiao et al., 1997); a nested urban and regional scale air quality prediction modeling system was developed and applied to investigate ozone pollution in Taiwan (Wang et al., 2001). Although important advances have taken place in air quality modeling, large uncertainties still remain, which are related to inaccurate and/or incomplete emission inventories, poorly represented initial and boundary conditions and missing or poorly parameterized physical and chemical processes (Carmichael et al., 2008a).

Furthermore, many models used to study air quality in Asia have been developed in other regions (e.g., USA and Europe), and the assumptions and parameterizations included in these models may not be applicable to the Asian environment. In order to develop a common understanding of model performance and uncertainties in Asia, and to further develop the models for Asian applications, a model inter-comparison study was initiated, i.e., Model Inter-Comparison Study for Asia Phase I (MICS-Asia I), in 1998 during a workshop on Transport of Air Pollutants in Asia in Austria. The focus of MICS-Asia Phase I was to study long-range transport and deposition of sulfur within Asia in support of on-going acid deposition studies. Eight long-range transport models from six institutes in Korea, Japan, Denmark, the USA, and Sweden

participated in MICS-Asia I. Multi-model results of sulfur dioxide (SO_2) and sulfate concentrations, and wet deposition amounts in January and May 1993 were compared with surface observations in East Asia (Carmichael et al., 2002). Source-receptor relationships and how model structure and parameters affect model performance were also discussed during this phase (Carmichael et al., 2002). In 2003, MICS-Asia Phase II was initiated to include more species, including nitrogen compounds, ozone and aerosols. The study period was expanded to cover two different years and three different seasons, and global inflow to the study domain was also considered (Carmichael et al., 2008b). Nine modeling groups from Korea, Hong Kong, Japan, the USA, Sweden, and France participated in this phase. Seven topics (i.e., ozone and related precursors, aerosols, acid deposition, global inflow of pollutants and precursors to Asia, model sensitivities to aerosol parameterization, analysis of emission fields, and detailed analyses of individual models) were discussed and published in a special issue of Atmospheric Environment (Carmichael et al., 2008b).

In 2010, MICS-Asia phase III was launched and three topics for this phase were decided during the first and second Workshop on Atmospheric Modeling in East Asia. Phase III aims to evaluate strengths and weaknesses of current air quality models and provide techniques to reduce uncertainty in Asia (Topic 1), to develop a reliable anthropogenic emission inventory in Asia (Topic 2), and to evaluate aerosol-weather-climate interactions (Topic 3). Various multi-scale models participated in this phase and the study periods range from year to month depending on study topics. This phase uses data from the Acid Deposition Monitoring Network in East Asia (EANET), in addition to new observations related to atmospheric chemistry in the region. An important advance to this phase is the inclusion of multiple online-coupled chemistry-meteorology models to investigate aerosol-weather-climate interactions, which is the target of

topic 3. On-line coupled models are playing important roles in air quality, meteorology and climate applications, but many important research questions remain (Baklanov et al., 2017).

The influences of aerosols on meteorology, e.g., radiation, temperature, boundary layer heights, winds, etc. and $PM_{2.5}$ concentrations have been examined in previous studies using different online coupled models (Gao et al., 2016a, 2016b; Han et al., 2012; Tao et al., 2015, 2016; Wang et al., 2014; Zhang et al., 2010). In general, there are two ways of online coupling: online integrated coupling (meteorology and chemistry are simulated using the same model grid, and one main time step is used to integrate) and online access coupling (meteorology and chemistry are independent but data are exchanged on a regular basis) (Baklanov et al., 2014). These two different coupling ways can lead to uncertainties in the results of aerosol-weather-climate interactions. Even using the same coupling way, different parameterizations in different online models causes uncertainties as well. Thus, it is important to inter-compare how different online models simulate aerosol-weather-climate interactions.

This paper presents and overview of the MICS-ASIA III Topic 3, serving as the main repository of the information linked to Topic 3 simulations and comparisons. This paper is organized as follows: in Section 2, we provide the inter-comparison framework of Topic 3, including the participating models, emissions, boundary conditions, observational data, and analysis methodology. Section 3 presents the general descriptions of the study periods and Section 4 presents comparisons and discussions focused on the results related to the meteorological and air pollution conditions during the January 2010 heavy haze episode. The results of January 2013 haze episode and detailed analysis of the direct and indirect effects will be presented in a companion paper.

Atmos. Chem. Phys. Discuss., https://doi.org/10.5194/acp-2017-731
Manuscript under review for journal Atmos. Chem. Phys.
Discussion started: 5 September 2017

2 Inter-comparison framework

In North China, severe aerosol pollution frequently happens and attracts enormous interests from both public and scientific communities (Cheng et al., 2016; Gao et al., 2015, 2016a, 2016b, 2016c, 2017). Two winter months in which severe haze episodes happened in North China were selected as the study periods for Topic 3. During these two months, maximum hourly $PM_{2.5}$ concentration in urban Beijing reached ~500 μg/m^3 and 1000μg/m^3, respectively. Compared to the China Grade 1 24-h $PM_{2.5}$ standard (35μg/m^3), daily mean $PM_{2.5}$ concentrations in urban Beijing exceeded this standard for 20 days and 27 days within these two months, respectively. The dramatically high aerosol loadings during these two hazy months substantially affected radiation transfer, and provide a good opportunity to study the aerosol effects on weather, air quality and climate. In this study, the participants were required to use common emissions to predict air quality during these two months and submit requested model variables. The emissions were placed on a publicly accessible website. Six modeling groups submitted results for Topic 3. In this section, we briefly describe these models and their configurations, introduce the emission inventories (including anthropogenic, biogenic, biomass burning, air and ship, and volcano emissions), observational datasets, and describe the analysis methodology.

2.1 Participating models

Table 1 summarizes the characteristics of the participating models. These models include: one application of the Weather Research Forecasting model coupled with Chemistry (WRF-Chem, Grell et al., 2005) by Pusan National University (PNU) (M1), one application of the WRF-Chem model by the University of Iowa (UIOWA) (M2), two applications (two domains: 45km and 15km horizontal resolutions) of the National Aeronautics and Space Administration (NASA)

Unified WRF (NU-WRF, Peters-Lidard et al., 2015; Tao et al., 2013) model by the Universities Space Research Association (USRA) and NASA's Goddard Space Flight Center (M3 and M4), one application of the Regional Integrated Environment Modeling System with Chemistry (RIEMS-Chem, Han et al., 2010) by the Institute of Atmospheric Physics (IAP), Chinese Academy of Sciences (M5), one application of the coupled Regional Climate Chemistry Modeling System (RegCCMS, Wang et al., 2010) from Nanjing University (M6), and one application of the coupled WRF-CMAQ (Community Multiscale Air Quality) model by the University of Tennessee at Knoxville (UTK) (M7). These models are all online coupled, which enables aerosol-weather-climate interactions. Domain setting of each model application is shown in Figure 1. The domains of M2, M5, and M6 (UIOWA, IAP, and NJU in Figure 1) cover most areas of East Asia, including China, North Korea, South Korea, Japan, Mongolia, and north parts of Southeast Asia. M1, M3 and M7 domains (PNU, NASA D01 and UTK) include more countries in Southeast and South Asia. M4 (NASA D02) covers east China, Korea and Japan. The horizontal model resolutions of these applications range from 15km to 60km (Table 1). Model vertical resolutions vary from 16 to 60 layers (Table 1) and the set model top pressures range from 100mb to 20mb.

Gas phase chemistry and aerosol modules are key components of chemical transport models. Although the WRF-Chem and NU-WRF models were applied at three institutes (PNU, UIOWA, and NASA), different gas phase chemistry and aerosol modules were used. At PNU (M1), the RACM-ESRL (Regional Atmospheric Chemistry Mechanism, Earth System Research Laboratory) gas phase chemistry coupled with MADE/VBS (Modal Aerosol Dynamics Model for Europe/Volatility Basis set) aerosol module was used. RACM was developed based on Regional Acid Deposition Model (RADM2) to simulate regional atmospheric chemistry

(Stockwell et al., 1997) (including 237 reactions) and the rate coefficients were updated in RACM ESRL version (Kim et al., 2009). MADE uses 3 log-normal modes (Aitken, accumulation, coarse) and simulates major aerosol compositions, including sulfate, ammonium, nitrate, sea-salt, black carbon (BC), and organic carbon (OC). In addition, the VBS method was implemented to simulate secondary organic aerosols (SOA). At the University of Iowa (M2), CBMZ (Carbon-Bond Mechanism version Z) gas phase chemistry coupled with an 8 bin MOSAIC (Model for Simulating Aerosol Interactions and Chemistry) aerosol module was applied. CBMZ (Zaveri and Peters, 1999) extends the original CBM4 mechanism to function properly at larger spatial and longer timescales. The augmented CBMZ scheme includes 67 species and 164 reactions. MOSAIC considers major aerosol species at urban, regional and global scales, including sulfate, nitrate, ammonium, sodium, chloride, EC, and other unspecified inorganic species (such as inert minerals, trace metals, and silica) (Zaveri et al. 2008). MOSAIC includes some aqueous reactions but no SOA formation. At NASA, the GOCART aerosol model (Chin et al., 2002) was coupled to RADM2 gas phase chemistry, and incorporated into the NU-WRF model (M3 and M4) to simulate major tropospheric aerosol species, including sulfate, BC, OC, dust, and sea-salt. In this aerosol model, 10% of organic compounds from the volatile organic compounds (VOCs) emission inventory are assumed to be converted to SOA (Chin et al., 2002).

Both the RIEMS-Chem model from IAP (M5) and the RegCCMS model from NJU (M6) used CBM4 to calculate gas phase chemistry (Gery et al., 1989). The CBM4 version incorporated in RIEMS-Chem (M5) includes 37 species and 91 reactions, and aerosols in RIEMS-Chem include sulfate, nitrate, ammonium, BC, OC, SOA, 5 bins of soil dust, and 5 bins of sea salt (Han et al., 2012). ISORROPIA (Nenes et al., 1998) is coupled to RIEMS-Chem to treat thermodynamic

equilibrium process and to simulate inorganic aerosols. SOA production from primary anthropogenic and biogenic VOCs is calculated using a bulk aerosol yield method according to Lack et al. (2004). A lognormal size distribution is assumed for inorganic aerosols, BC, and OC, with median radius of 0.07 mm, 0.01 mm, and 0.02 mm, and geometric standard deviation of 2.0, 2.0, and 2.2, respectively. The schemes for soil dust deflation and sea salt generation were from Han et al. (2004), which used 5 size bins (0.1-1.0, 1.0-2.0, 2.0-4.0, 4.0-8.0, 8.0-20.0μm) to represent dust and sea salt size distribution. The refractive indices of aerosol components were mainly derived from the OPAC (Optical Properties of Aerosols and Clouds) database. Aerosol extinction coefficient as well as single scattering albedo and asymmetry factor are calculated by a Mie-theory based parameterization developed by Ghan and Zaveri (2007), which has a high computational efficiency with similar degree of accuracy compared with complete Mie code. An internal mixture of aerosols was assumed in this region of large emissions. A method known as kappa (k) parameterization (Petters and Kreidenweis, 2007) was adopted to represent the aerosol hygroscopic growth.

The version of CBM4 implemented in RegCCMS (M6) consists of 36 reactions (4 photolysis reactions) and 20 species (Wang et al., 2010). RegCCMS also used ISORROPIA to calculate inorganic aerosols (Wang et al., 2010). For implementation of aerosol effects, sulfate radiative properties were treated following Kiehl and Briegleb (1993), OC were assumed to have the same properties as sulfate, and the wavelength-dependent radiative properties of BC follows Jacobson (2001).

M7 applied SAPRC 99 coupled to the sixth-generation CMAQ aerosol module (AE6) to simulate gas phase chemistry and aerosol formation The SAPRC99 mechanism implanted within the CMAQ model has 88 species and 213 chemical reactions (Carter, 2000a,b). AE6 aerosol

mechanism is to couple with WRF. There are seven components including water soluble mass, water insoluble mass, elemental carbon, sea salt, water, diameters and standard deviations passed to WRF. Many previous studies have underscored that the choice of gas phase mechanism and aerosol models are of great importance for simulating air pollutants (Knote et al., 2015; Zhang et al., 2012). The different gas phase chemistry and aerosol modules used in the participating models are expected to yield notable differences in performances, which are shown later in section 4.

Although the WRF-Chem and NU-WRF models were applied at three institutes (PNU, UIOWA, and NASA), different physics configurations are also used. Table S1 compares the used microphysics, radiation, boundary layer, cumulus clouds, and surface schemes used by WRF-Chem and NU-WRF applications. Both aerosol-radiation and aerosol-microphysics are included in these applications, but different used microphysics (M1 uses Lin, M2 uses Morrison and M3 uses Goddard) and radiation (M1 and M2 use RRTMG, but M3 uses Goddard) schemes will lead to differences in estimates in aerosol direct and indirect effects, in addition to the differences in simulated aerosols.

2.2 Emissions

The accuracy of air quality modeling results highly depends on the quality and reliability of emission inventory. Accordingly, a new Asian emission inventory was developed for MICS-III by integrating state-of-the-art national/regional inventories to support this model inter-comparison study (Li et al., 2017). This is the major theme of MICS-ASIA III Topic 2. These emissions, along with biogenic emissions, biomass burning emissions, emissions from air and

246 ship, and volcano emissions were used. This section offers some basic descriptions of these
247 provided emissions.

248 **2.2.1 Anthropogenic emissions**

249 The state-of-the-art anthropogenic emission inventory for Asia (MIX) was developed by
250 incorporating five inventories, including the REAS inventory for Asia developed at the Japan
251 National Institute for Environmental Studies (NIES), the MEIC inventory for China developed at
252 Tsinghua University, the high resolution ammonia (NH_3) emission inventory in China developed
253 at Peking University, the Indian emission inventory developed at Argonne National Laboratory
254 in the United States, and the CAPSS Korean emission inventory developed at Konkuk University
255 (Li et al., 2017). This MIX inventory includes emissions for ten species, namely SO_2, nitrogen
256 oxides (NO_x), carbon monoxide (CO), non-methane volatile organic compounds (NMVOC),
257 NH_3, PM_{10}, $PM_{2.5}$, BC, OC, and carbon dioxide (CO_2). NMVOC are provided with CB-05 and
258 SAPRC-99 speciation datasets. Emissions of these species were prepared for years 2008 and
259 2010 in monthly temporal resolution and 0.25 degree spatial resolution. Weekly/diurnal profiles
260 were also provided. Five sectors were considered, namely industry, power generation, residential
261 sources, transportation and agriculture. Figure 2 shows the spatial maps of these ten species for
262 January 2010. Emissions of most of these species exhibit similar spatial patterns, with enhanced
263 values in east China and lower values in north and south India. Emissions of NH_3 display a
264 different spatial distribution, with pronounced values in India and lower values in north China
265 (Figure 2). More detailed description of this emission inventory is documented in Li et al.
266 (2017).

267 **2.2.2 Biogenic emissions**

Terrestrial ecosystems generate miscellaneous chemical species, including volatile and semi-volatile compounds, which play important roles in atmospheric chemistry and are the largest contributor to global annual flux of reactive volatile organic compounds (VOCs) (Guenther et al., 2006). For MICS-ASIA III, hourly biogenic emissions were provided for the entire year of 2010 using the Model of Emissions of Gases and Aerosols from Nature (MEGAN) version 2.04 (Guenther et al., 2006). The variables that drive MEGAN include land cover information (plant function type, leaf area index) and weather condition, which includes solar transmission, air temperature, humidity, wind speed, and soil moisture. In the preparation of MEGAN biogenic emissions, land cover information is taken from the NASA MODIS products, and weather condition are calculated using WRF simulations. Figure S1 shows biogenic emissions of some selected species (isoprene and HCHO) for January 2010. High biogenic emissions are found in south Asia during winter, including India, south China, and Southeast Asia, where solar radiation, air temperature and vegetation covers are relatively higher than in northern regions. Some models used these emissions directly. Others internally calculated the biogenic emissions on-line with the model predicted meteorology using the MEGAN model.

2.2.3 Biomass burning emissions

Biomass burning in the tropics is a strong contributor to air pollutants, and extensive biomass burning in Asia, particularly Southeast Asia, exerts a great influence on air quality (Streets et al., 2003). For MICS-ASIA III, biomass burning emissions were processed by re-gridding the Global Fire Emissions Database version 3 (GFEDv3) (0.5 by 0.5 degree). GFED fire emissions are estimated through combining satellite-detected fire activity and vegetation productivity information. Carbon, dry matter, CO_2, CO, CH_4, hydrogen, nitrous oxide, NO_x, NMHC, OC, BC, $PM_{2.5}$, total particulate matter and SO_2 emissions are estimated in monthly temporal resolution.

Figure S2 shows the gridded biomass burning emissions for January 2010. Biomass burning activity is highest in Cambodia and some areas of Myanmar and north of Thailand (Figure S2), and the peak emission season is spring. Although it has been concluded that biomass burning could significantly contribute to aerosol concentrations in China, the contribution is limited for Topic 3 study since the focused region is North China where biomass burning emissions are negligible during cold winter (Gao et al., 2016a).

2.2.4 Volcanic SO_2 emissions

Volcanoes are important sources of various sulfur and halogen compounds, which play crucial roles in tropospheric and stratospheric chemistry. It is estimated that SO_2 emitted from volcanoes account for about 9% of the total worldwide annual SO_2 flux (Stoiber et al., 1987). The Asia-Pacific region is one of the most geologically unstable regions in the world where many active volcanoes are located. During MICS-ASIA Phase II, the volcano SO_2 emissions had already been provided for chemical transport models (Carmichael et al. 2008b). Volcano SO_2 emissions were provided, with a daily temporal resolution. In January, some volcanoes in Japan are very active, such as Miyakejima (139.53ºE, 34.08ºN, and 775m above sea level) and Sakurajima (130.65ºE, 31.59ºN, 1117m above sea level).

2.2.5 Air and Ship emissions

Fuel burning in aircraft and ship engines produces greenhouse gases and air pollutants. The shipping and aircraft emissions used are based on HTAPv2 emission inventory (0.1 by 0.1 degree) for year 2010 (Janssens-Maenhout et al., 2015), provided on an annual basis. Aircraft emissions include three parts: landing and takeoff (LTO), climbing and descent (CDS), and cruise (CRS). Aircraft emission hot spots are mostly located in Japan, and Beijing, Yangtze

River Delta (YRD) and Pearl River Delta (PRD) in China (Figure S3). East China Sea, sea around Japan and Singapore exhibit high shipping emissions due to active shipping transportation (Figure S3). It is estimated that international shipping contributed about 10% to the global SO_2 emissions, and together with aviation contribute more than 10% of global NO_x emissions (Janssens-Maenhout et al., 2015).

2.3 Boundary conditions

To predict more realistic spatial and temporal variations of air pollutants, boundary conditions from global chemical transport models are necessary to drive regional chemical transport models (Carmichael et al., 2008b). Simulations of three global chemical transport models (i.e., CHASER, GEOS-Chem and MOZART) were provided as boundary conditions for MICS-ASIA III. CHASER was developed in Japan to simulate the O_3-HO_x-NO_x-CH_4-CO photochemical system and its effects on climate (Sudo et al., 2002). GEOS-Chem was developed in the USA to simulate tropospheric chemistry driven by assimilated meteorology (Bey et al., 2001). In addition, the National Center for Atmospheric Research (NCAR) also provides global simulations of atmospheric chemistry (MOZART model) and an interface to convert them to WRF-Chem boundary conditions (Emmons et al., 2010), and NASA provides global aerosol distributions using the global GOCART chemistry model (Chin et al., 2002). GEOS-Chem was run with 2.5ºx2º resolution and 47 vertical layers and CHASER model was run with 2.8ºx2.8º and 32 vertical layers. 3 hourly-average fields of gaseous and aerosols were distributed to all participants. The MOZART-4 simulations were also configured at the horizontal resolution of 2.8ºx2.8º, but with 28 vertical levels. NASA GOCART was configured at the same resolution as GEOS-5 meteorology (1.25ºx1º). As listed in Table 1, M1 used climatological data from the NOAA Aeronomy Lab Regional Oxidant Model (NALROM), while M2 used boundary

conditions from the MOZART-4 (provided from the NCAR website). M3 and M4 used MOZART-4 as boundary conditions for gases and used GOCART as boundary conditions for aerosols. M6 also used fixed climatology boundary conditions, and M5 and M7 used GEOS-Chem outputs as boundary conditions. Even though the same global model is used as boundary conditions, the treatments of inputs might differ in details, which might lead to considerable dissimilarities. In MICS-ASIA II, Holloway et al. (2008) discussed the impacts of uncertainties in global models on regional air quality simulations.

2.4 Observation data

Historically, the lack of reliable air quality measurements in Asia has been a bottleneck in understanding air quality and constraining air quality modeling in Asia. Beginning MICS-ASIA II, observational data from Acid Deposition Monitoring Network in East Asia (EANET) has been used to evaluate model performance. EANET was launched in 1998 to address acid deposition problems in East Asia, following the model of the Cooperative Program for Monitoring and Evaluation of the Long-range Transmission of Air pollutants in Europe (EMEP). As of 2010, there are 54 wet deposition sites and 46 dry deposition sites in 13 participating countries. Quality assurance and quality control measures are implemented at the national levels and in the Inter-laboratory Comparison Project schemes to guarantee high quality dataset. EANET supported current activities of MICS-ASIA III, and provided measurements in 2010 to all modeling groups. More information about EANET dataset can be found in http://www.eanet.asia/.

In addition to EANET data, measurements of air pollutants and aerosol optical depth (AOD) collected at the Campaign on Atmospheric Aerosol Research network of China (CARE-China)

(Xin et al., 2015) network were also used. Previous successful networks in Europe and the United States underscored the importance of building comprehensive observational networks of aerosols in China to get better understanding of the physical, chemical and optical properties of atmospheric aerosols across China. As the first comprehensive attempt in China, CARE-China was launched in 2011 by Chinese Academy of Sciences (CAS) (Xin et al., 2015). Before launching this campaign, CAS had already been measuring air pollutants and AOD at some CARE-China sites. Table 2 summaries the locations and characteristics of the CARE-China measurements for January 2010. Air quality measurements include concentrations of $PM_{2.5}$, PM_{10}, SO_2, NO_2, NO, CO, O_3.

In addition, AOD from Aerosol Robotic Network (AERONET) (https://aeronet.gsfc.nasa.gov/) and operational meteorological measurements (near surface temperature, humidity, wind speed and downward shortwave radiation) in China and atmospheric sounding data in Beijing were used. AERONET provides long-term, continuous, readily accessible and globally distributed database of spectral AOD, inversion products and precipitable water. AOD data are calculated for three quality levels: Level 1.0 (unscreened), Level 1.5 (cloud screened), and Level 2.0 (cloud screened and quality assured) (Holben et al., 1998). The locations and characteristics of the AERONET measurements are also summarized in Table 2. In-situ measurements of meteorological data from standard stations in China are operated by China Meteorological Administration (CMA) and different levels of data, including daily, monthly, and annually, are open to the public (http://data.cma.cn/en). The locations of all used observational sites are marked in Figure S4, Figure S5 and Figure S6.

The meteorology measurements (locations are shown in Figure S4) were averaged and compared with model results that averaged across those locations. The radiation measurements were

averaged and compared against model results in North China and South China (locations are shown in Figure S5), separately. The CARE-China, AERONET and EANET measurements (locations are shown in Figure S5 and S6) were compared against model results site by site, and model ensemble mean values were made by averaging all model results.

2.5 Analysis methodology

All groups participating in Topic 3 were requested to simulate meteorology, air quality, radiative forcing and effects of aerosols over the Beijing-Tianjin-Hebei region of east China during two periods: January 2010 and January 2013. Simulations were designed to evaluate radiative and microphysical feedbacks, together and separately, relative to simulations without feedbacks. Each group was requested to submit the following fields from their simulations.

(1) hourly mean meteorology:

(a) air temperature and water vapor mixing ratio at 2m above ground (T2, Q2), wind speed at 10m above groud (WS10), and shortwave radiation flux (Wm-2) at the surface;

(b) above variables (except shortwave radiation flux) at 1km and 3km above ground.

(2) hourly mean concentrations:

(a) SO_2, NO_x, CO, O3, $PM_{2.5}$, PM_{10} and sulfate, nitrate, ammonium, BC, OC and dust in $PM_{2.5}$;

(b) above variables at 1km and 3km above ground.

(3) hourly mean AOD, aerosol direct radiative forcings at the surface, top of the atmosphere (TOA) and inside the atmosphere (single scattering albedo is an option for participants).

(4) Hourly mean integrated liquid water, cloud optical depth.

401 (5) Changes in T2, Q2, WS10 and $PM_{2.5}$ concentrations at the surface due to both direct and
402 indirect aerosol's effects.

403 We calculated multiple model evaluation metrics, including correlation coefficient (r), root mean
404 square error (RMSE), mean bias error (MBE), normalized mean bias (NMB), mean fractional
405 bias (MFB) and mean fractional error (MFE). The equations are presented in supplemental
406 information.

407

408 3 General description of meteorology and haze during the study periods

409 Winter haze events are frequently happening in east China, which is partially due to the stagnant
410 weather conditions in winter. Here we present general descriptions of the meteorological
411 conditions during the selected two January months using the NCEP/NCAR reanalysis products.
412 Figure 3 (a, b) display the monthly mean T2 (temperature at 2m) and W10 (wind speeds at 10m)
413 for January 2010 and January 2013, respectively. For both periods, WS10 were very weak in
414 eastern and central China regions. T2 in Mongolia region was relatively higher for January 2013.
415 Historical analyses have shown that cold conditions are usually associated with strengthened
416 Siberian High (Gong and Ho, 2002), and relatively higher T2 and more weakened Siberian High
417 (Figure 3 (c, d)) during January 2013 led to weaker winter monsoon winds and higher pollution
418 levels. The relatively weaker Siberian High during January 2013 compared to January 2010 is
419 also shown in the sea level pressures (Figure 3 (c, d)). The Siberian High center was about
420 1037mb during January 2013, lower than that (1040mb) during January 2010. Figure 3 (c, d)
421 show that there was no significant precipitation in North China and heavy rainfall only occurred
422 in Southeast Asia regions. During cold winters, northern China burns coal for heating, generating

more emissions. Under stagnant weather conditions, haze episodes are easily triggered. It was reported that January 2013 was the haziest month in the past 60 years in Beijing, and instantaneous $PM_{2.5}$ concentration exceeded 1000μg/m^3 in some areas in Beijing. Winter haze also happened from 16 to 19 January in 2010. High concentrations of aerosols during these two study periods provide great opportunity to study aerosol-radiation-weather interactions.

4 Results and discussions

In this section, we present some major features of model performances in meteorological and chemical variables for the January 2010 period. Detail analysis of feedbacks and radiative forcing are presented in MICS-ASIA III companion papers. Heavy haze occurred over broad regions of East China in January 2010. The plots of observed meteorological variables and $PM_{2.5}$ in Beijing show the general situation (Figure 4). Elevated $PM_{2.5}$ occurred during three periods separated in time by roughly one week (January 8, 16 and 26). The major event occurred during January 15-21. The events occurred during periods of low wind speeds, and increasing temperature and relative humidity. The high $PM_{2.5}$ concentrations during January 15-21 also greatly reduce the downward shortwave radiation. Below we evaluate how well the models predict these features.

4.1 Evaluation of meteorological variables

Air quality is affected by not only emissions, but also meteorological conditions. Meteorology affects air quality through altering emissions, chemical reactions, transport and deposition processes (Gao et al., 2016b). Thus, it is important to assess how well these participating models

reproduced meteorological variables. The predicted temperature at 2m high (T2), water vapor mixing ratio at 2m (Q2), wind speed at 10m high (WS10) and daily maximum downward shortwave radiation (SWDOWN) were evaluated against near surface observations at the CMA sites.

Figure 5 (a-c) shows the comparisons between simulated and observed daily mean T2, Q2 and WS10 averaged over stations in East China (locations are shown in Figure S4) during January 2010, along with multi-model ensemble mean and observation standard deviation. The calculated correlation coefficients between models and observations are also shown in Figure 5 and other calculated model evaluation metrics are summarized in Table 3. In general, the simulated magnitudes and temporal variations of T2 and Q2 show high order of consistencies with observations, with correlation coefficients ranging from 0.88 to 1. For T2, models tend to have a cool bias; M1 and M2 have the lowest RMSE (0.64 and 0.68), lowest MBE (-0.19 and -0.60) and lowest NMB (-0.07% and -0.22%) values (Table 3). For Q2, most models tend to slightly overestimate; M1 and M2 have the best performance, with the lowest RMSE (0.14 and 0.10), lowest MBE (0.02 and -0.01), and lowest NMB (0.84% and -0.55%) values (Table 3).

Simulated WS10 exhibit larger diversity of results. All models tend to overestimate WS10, with MBE ranging from 0.15m/s to 2.37m/s. Overestimating wind speeds under low wind conditions is a common problem of current weather forecasting models, and many factors, including errors in terrain data and reanalysis data, relatively low horizontal and vertical model resolutions, as well as poorly parameterized urban surface effect, contribute to these overestimations. From the calculated RMSE, MBE, and NMB listed in Table 3, M2, M5 and M7 show better skills in capturing WS10. In addition, the multi-model ensemble mean show the lowest RMSE for Q2, and also better skills than most models for T2 and WS10. The correlation coefficients between

multi-model ensemble mean and observations are 0.99, 0.99 and 0.98 for T2, Q2 and WS10, respectively.

The accuracy of radiation predictions is of great significance in evaluating aerosol-radiation-weather interactions. We evaluated simulated daily maximum SWDOWN averaged over sites in northern China and southern China separately in January 2010 against observations. The locations of the radiation sites are shown in Figure S5. As shown in Figure 5 (d), over stations in northern China, all models except M6 and M7 reproduce daily maximum SWDOWN well, with correlation coefficients ranging from 0.72 to 0.94. SWDOWN decreases under conditions of high PM, as shown for example on January 9 and 15-21. This is one of the important reasons for coupled air quality and meteorology modeling, as they can account for this effect of aerosols. It is worth noting that most models predict higher daily maximum SWDOWN compared to observations when severe haze happened in the North China Plain (16-19 January 2010), indicating aerosol effects on radiation might be underestimated. Over southern China sites (Figure 5e), M6 and M7 show a better consistence with observations than over northern China sites. According to the calculated RMSE listed in Table 3, M3 and multi-model ensemble mean exhibit relatively better performance in capturing the observed time series of daily maximum SWDOWN in both northern China and southern China.

The above comparisons show that T2 and Q2 are reproduced well by the participating models, and WS10 is overestimated by all models. Emery et al. (2001) proposed that excellent model performance would be classified as wind speed RMSE smaller than 2 m/s, and wind speed bias smaller than 0.5 m/s. Based on the calculated RMSE and MBE of WS10 shown in Table 3, RMSE values from all models match the proposed RMSE threshold but MBE values are higher than 0.5 m/s. The vertical distributions of temperature, water vapor mixing ratio and wind speeds

were also validated against atmospheric sounding data in Beijing at 1km and 3km (Figure S7, averaged at 00:00 and 12:00 UTC) (http://weather.uwyo.edu/upperair/sounding.html). The magnitudes of temperature, water vapor mixing ratio and wind speeds from different models are generally consistent with each other at 1km and 3km, but variations are larger near surface.

4.2 Evaluation of air pollutants

Figure 6 displays the daily averaged predicted and observed SO_2, NO_x, CO, O_3, $PM_{2.5}$, and PM_{10} at the Beijing station, along with the observation standard deviation (locations are shown in Figure S6). Comparisons for the Tianjin, Shijiazhuang and Xianghe sites are shown in Figure S8-S10. M6 only provided SO_2, NO_x concentrations, so it is not only shown in the plots of CO, O_3, $PM_{2.5}$, and PM_{10}. The observed and predicted primary pollutants and $PM_{2.5}$ and PM_{10} show the same monthly variations with elevated values at roughly weekly intervals, with the largest event occurring during January 15-21. For example, as shown in the comparisons of SO_2 concentration, the temporal variations are reproduced well by all the models, but peak values are overestimated or underestimated by some models. Based on the calculated MBE values shown in Table 4, all models except M2 tend to underestimate SO_2 in Beijing. M1 shows the highest correlation (0.90) with SO_2 observations in the Beijing site, and most other models show similar good correlations. The multi-model ensemble mean shows a better agreement with observations with a higher correlation of 0.92, and it falls within the range shown with standard deviation error bar. In general, the predictions for NO_x capture the main features in the observations, with slightly less skill than for the SO_2 prediction. The calculated correlation coefficients for NO_x from different models are close to each other, ranging from 0.63 to 0.88. M2 and M5 predict higher NO_x concentrations than observations and other models (MBE in Table 4). All models overestimate NO_x concentration in Shijiazhuang (Figure S8), suggesting NO_x emissions in

513 Shijiazhuang might be overestimated in the MIX emission inventory. All models are consistent
514 with each in CO predictions.

515 $PM_{2.5}$ concentrations are well modelled, with high correlation coefficients ranging from 0.87 to
516 0.90 in Beijing, from 0.83 to 0.93 in Tianjin, and from 0.74 to 0.91 in Xianghe. The correlation
517 coefficient of the multi-model ensemble mean for $PM_{2.5}$ reaches 0.94 (Table 4), better than any
518 individual model. The performances of all participating models in reproducing PM_{10} variations
519 are not as good as reproducing $PM_{2.5}$. M1 and M2 overestimate PM_{10} concentrations, and other
520 models underestimate PM_{10} concentrations (MBE in Table 4). These biases are probably related
521 to different treatments of primary aerosols and anthropogenic dust in the models.

522 The models showed the poorest skill in predicting ozone. All models exhibit different
523 performances in simulating ozone concentrations, and the correlation coefficients between
524 models and observations can reach negative values (Figure S8). M3 and M4 tend to overestimate
525 ozone concentrations, M2 slightly overestimates it, and M1, M5, and M7 slightly underestimate
526 it (MBE in Table 4). According the calculated RMSE in Table 4, M1 and M7 shows relatively
527 better performance in modeling ozone variations. Although WRF-Chem and NU-WRF models
528 were applied at three institutions, different gas phase chemistry schemes were used, which leads
529 to these diversities among predicted ozone concentrations. The impacts of gas phase chemical
530 mechanisms on ozone simulations have been investigated in Zhang et al. (2012); but under high
531 photochemical conditions. The results presented here winter conditions with slower
532 photochemistry in general and where hazy conditions further reduce photochemistry through
533 diming effects.

Figure 7 shows the comparisons between modeled and observed ground level daily averaged concentrations of SO_2, NO_x, O_3 and PM_{10} during January 2010 at the Rishiri site in Japan from EANET. The locations of used EANET sites are marked in Figure S6. Comparisons at other EANET sites are shown in Figure S11-S14. The models are able to predict the major features in the observations. For example, low values of most pollutants are observed (and predicted) during the first half of the month, followed by elevated values, which peak on January 21. For SO_2, most models show similar capability in producing the temporal variations in observations with slight underestimation (MBE in Table 5). According to the calculated RMSE averaged over all the EANET sites, M2 and the multi-model ensemble mean performed the best. For NO_x, the multi-model ensemble mean shows lower RMSE than any individual model (Table 5). Similar to the comparisons over CARE-China sites, large discrepancies exist in ozone predictions, but the model ensemble mean still shows lowest RMSE for ozone predictions. PM_{10} concentrations are largely underestimated by M1 (largest negative MBE: -21.03ug/m^3) and overestimated by M5 (highest positive MBE: 3.77ug/m^3) (Table 5), which could also be related to differences in the way sea-salt emissions are treated in the various models.

4.3 $PM_{2.5}$ and $PM_{2.5}$ chemical composition distribution

Haze pollution is characterized by high loadings of $PM_{2.5}$, thus accurately predicting $PM_{2.5}$ and its chemical compositions are crucial to understand haze pollution and to provide insightful implications for controlling haze in China. The accuracy of predicting $PM_{2.5}$ chemical composition is also of great importance in estimating aerosol-radiation interactions. For example, black carbon absorbs shortwave radiation, whereas sulfate and organic carbon mostly scatter radiation. Due to different implementations of chemical reactions in the models, predicted $PM_{2.5}$ chemical compositions from participating models differ largely. Figure 8 and Figure 9 show the

predicted monthly mean concentrations of sulfate, nitrate, ammonium, BC and OC in $PM_{2.5}$ from all participating models for January 2010.

M1, M2, M3, M4 and M7 all predict quite low sulfate concentrations in east China, but with considerably enhanced sulfate in southwest areas of China and west areas of India. M5 and M6 shows similar spatial patterns of sulfate except that M6 produces higher concentrations. The chemical production of sulfate is mainly from gas-phase oxidation of SO_2 by OH radicals and aqueous-phase pathways in cloud water. In cloud water, dissolved SO_2 can be oxidized by O_3, H_2O_2, Fe(III), Mn(II), and NO_2 (Seinfeld and Pandis, 2016). Most chemical transport models have included the above gas phase oxidation of SO_2 by OH and oxidation of SO_2 by O_3 and H_2O_2 in aqueous phase. Under hazy conditions, radiation is largely reduced due to aerosol dimming effects, and sulfate formation from gas phase and aqueous phase oxidation processes are slowed down, which tend to reduce sulfate concentration. However, field observations exhibit an increase in sulfate concentration during haze episode (Zheng et al., 2015), and Cheng et al. (2016) proposed that the reactive nitrogen chemistry in aerosol water could contribute significantly to the sulfate increase due to enhanced sulfate production rates of NO_2 reaction pathway under high aerosol pH and elevated NO_2 concentrations in the North China Plain (NCP) during haze periods. Wang et al. (2016) also pointed out the aqueous oxidation of SO_2 by NO_2 is key to efficient sulfate formation on fine aerosols with high relative humidity and NH_3 neutralization or under cloudy conditions. Besides, Zheng et al. (2015) suggested that heterogeneous chemistry on primary aerosols could play an important role in sulfate production and lead to increasing sulfate simulation during haze episodes. The above aqueous and heterogeneous processes are currently not incorporated in the participating models for this study, which might be responsible for the apparent under-predictions

of sulfate concentration (Figure 10). M5 also incorporated heterogeneous chemical reactions on aerosol surface (Li and Han, 2010), which enhances total sulfate production.

M1 and M5 predict relatively small nitrate and ammonium concentrations; while M2, M6 and M7 produces similar magnitudes and spatial patterns of nitrate. Nitrate formation involves both daytime and nighttime chemistry. During daytime, NO_2 can be oxidized by OH to form nitric acid (HNO_3), and by ozone to form NO_3. HNO_3 is easily removed by dry or wet deposition, but NO_3 is easily photolyzed back to NO_2. During nighttime, NO_3 is the major oxidant, which oxides NO_2 to form dinitrogen pentoxide (N_2O_5). Homogenous reaction of N_2O_5 with water vapor is possible but very slow while heterogeneous uptake of N_2O_5 onto aerosol particles has been identified as a major sink of N_2O_5 and an important contributor to particulate nitrate (Kim et al., 2014). The MOSAIC aerosol module (Zaveri et al., 2008) coupled with CBMZ gas phase chemistry in WRF-Chem already includs heterogeneous uptake of N_2O_5 since version v3.5.1 (Archer-Nicholls et al., 2014), which is the version used by M2, leading to the high production of nitrate. M7 also predict high nitrate concentrations, and the predicted lower nitrate concentrations from other models are probably due to missing aqueous phase and heterogeneous chemistry. M3 and M4 do not include the explicit nitrate and ammonium treatment but ammonium is implicitly considered in total $PM_{2.5}$ mass estimate.

The predicted ammonium concentrations are associated with the amounts of sulfate and nitrate, as shown by its similar spatial distribution to sulfate and nitrate. NH_3 neutralizes H_2SO_4 and HNO_3 to form aerosol, so its amount can affect the formation of sulfate, nitrate and ammonium. Since the same emission inventory was used, the amount of ammonia available for neutralizing will not vary greatly among these models. Thus, the rates of H_2SO_4 and HNO_3 production determines the amounts of ammonium. For example, the produced ammonium concentrations are

small in M1, similar to their sulfate and nitrate productions. High ammonium concentrations are predicted from M6, due to high productions of nitrate and sulfate (Figure 8).

The spatial distributions and magnitudes of predicted BC from all participating models are similar to each other as BC is a primary pollutant whose mass as BC is not impacted by chemical reactions. The concentrations of BC in the atmosphere are mainly influenced by PBL mixing and diffusion, aging, deposition and advection. Predicted BC from M2 and M7 are higher than from other models, which might be caused by different treatments of emission inventory (for example, how to distribute emissions to different vertical layers), horizontal grid interpolation, and/or different parameterizations for vertical diffusion, aging, deposition and advection.

The disparity among predicted OC concentrations is mainly associated with the different treatments of SOA production, given the POC prediction is generally consistent among models using the same emission inventory. The predicted OC concentrations from M1, M2, and M7 are close to each other. M1 uses SORGAM (Secondary Organic Aerosol Model) to simulate SOA, but M2 and M6 did not include any SOA formation mechanism. The similar magnitudes of OC from M1 and M2 suggest that SORGAM in M1 does not produce appreciable amounts of SOA, which is consistent with the findings in Gao et al. (2016a). Although SOA formation is implemented in M5, the production is relatively weak compared to M3 and M4. In the atmosphere, SOA is mainly formed from the condensation of semi-VOCs from oxidation of primary VOCs. An empirical 2-produt model (Odum et al., 1996) is often used to simulate SOA formation, but this method was reported to significantly underestimate measured SOA mass concentrations. Later, the volatility basis-set approach (Donahue et al., 2006) was developed to represent more realistically the wide range of volatility of organic compounds and more complex processes, and it was found to increase SOA production and to reduce observation-simulation biases in many regions with high emissions

(Tsimpidi et al., 2010) including east China (Han et al., 2016). It was also suggested that primary organic aerosols (POA) are semi-volatile and can evaporate to become SOA precursors, which promotes the understanding and improvements of SOA modeling (Li et al., 2011). In M5, the SOA production is calculated using a bulk yield method via Lack et al. (2004), in which the amount of SOA able to be produced from a unit of reacted VOC from anthropogenic and biogenic origins are used to represent SOA yields. However, the SOA concentration is highly dependent on the yield data. During haze episodes, photochemistry is reduced due to the aerosol dimming effect, thus aqueous reaction processes on aerosol water and cloud/fog water could become much more important in producing SOA as suggested in Cheng et al. (2016). The missing representation of such process in the participating models may partly account for the low values in the simulated SOA. In M3 and M4, SOA is treated by assuming that 10% of VOCs from terrestrial source are converted to OC (Chin et al., 2002), and these models produce high OC concentrations, with a major contribution from SOA. The 10% yield rate could be unrealistically high during hazy days because solar radiation was much reduced.

The different predictions of $PM_{2.5}$ chemical components lead to differences in $PM_{2.5}$ concentrations for January 2010, which are shown in the last row of Figure 9. Although spatial distributions of $PM_{2.5}$ from these models are similar, the underlying causes are different. M2, M3 and M5 simulated higher $PM_{2.5}$ levels in deserts of west China, which are contributed by dust deflation. M1 and M7 fail to produce high $PM_{2.5}$ concentrations in the deserts of west China, due to omission of dust emissions. M4 presented results in a smaller domain excluding west China. The enhanced $PM_{2.5}$ concentrations in Central China from M2 and M7 are caused by large nitrate production, as shown in Figure 8.

The differences in the predictions of aerosols composition discussed above can be seen clearly in the comparisons at the Beijing site on 13-23 January when a haze event occurred in the NCP (Figure 10). Also shown are the observed values. Most models fail to produce the observed high sulfate concentrations. Only M5 prediction is close to observation, and M6 predicts higher sulfate level. M2 and M7 predict reasonable nitrate concentrations. M3 and M4 largely overpredict OC during haze period, but other models tend to underpredict OC concentrations.

Figure 11 and 12 show the ensemble mean monthly averaged near-surface $PM_{2.5}$, $PM_{2.5}$ composition, along with the spatial distribution of the coefficient of variation. The coefficient of variation is defined as the standard deviation divided by the average (Carmichael et al., 2008), and larger values indicate lower consistency among models. Mean concentrations of $PM_{2.5}$ and $PM_{2.5}$ chemical compositions are high in Sichuan Basin and east China. High coefficient of variation are shown in North China for sulfate, and in most areas for nitrate and OC. The diversity in predictions of these species are caused by complexity of secondary formation and different treatments in models as discussed earlier. Higher consistency is shown for model BC with coefficient of variations less than 0.3 in most areas (Figure (h)). Coefficient of variations for $PM_{2.5}$ are also low in North China region, which is consistent with good performance of $PM_{2.5}$ predictions shown in above comparisons. However, the coefficient of variation can reach above 1.6 in northwestern regions, partially due to discrepancies in dust predictions.

4.4 Evaluation of AOD

AOD is an indication of aerosol pollution, which tells us how much sunlight is blocked from reaching the surface by suspended aerosols. We used the measurements of AOD at AERONET and CARE-China sites to evaluate how participating models perform in simulating AOD. In

669 WRF-Chem, AOD is usually calculated at 300, 400, 600 and 999nm, which can be converted to
670 AOD at other wavelengths based on Angstrom exponent relation (Schuster et al., 2006). The
671 submitted AOD from all models except M6 are at 550nm, and AOD from M6 are at 495nm. We
672 used Angstrom exponent relation (Schuster et al., 2006) to convert AOD from M6 at 495nm to
673 550nm, and all used AERONET and CARE-China AOD data to 550nm. The locations of
674 AERONET and CARE-China AOD measurement sites are shown in Figure S5. Daytime mean
675 AOD are calculated in pairwise manner and the comparisons and performance statistics are
676 shown in Figure 13, 14, and Table 6. On some days, data are missing because AOD cannot be
677 retrieved under serious pollution conditions (Gao et al., 2016a). On days with data, the variations
678 of AOD are captured well by all models. However, large disparities exist among models in the
679 simulated peak AOD values (factor of 2) at monitoring stations during the severe haze episode
680 on 15-20 January 2010 (Figure 13 and Figure 14). The participating models exhibit various skill
681 in simulating AOD temporal variation at different sites.

682 At CARE-China sites, M7 produces the best correlation coefficient R (0.83) among models at
683 Baoding and Beijing forest sites, M2 produces the highest R (0.86) at Cangzhou site, whereas
684 M5 shows the highest R (0.93) at the Beijing city site. At AERONET sites, M7 shows the
685 highest R (0.81) at Beijing, whereas M2 and M5 produce R as high as 0.91 at Xianghe site,
686 which is about 60km southeast of downtown Beijing. In terms of AOD magnitude, it's interesting
687 to note that during the severest haze days around 19 January 2010, M2 consistently simulates the
688 highest AOD among models, followed by M5 and M7, with the lowest AOD from M6, and other
689 models in the middle at the sites (Baoding, Beijing City, Beijing Forest, Cangzhou, Beijing,
690 Xianghe) in the north China plain (NCP). It is important to explore the causes for the disparities
691 in AOD predicitons.

AOD is calculated as the vertical integration of extinction coefficient, which is a function of particle mass extinction efficiency (extinction cross section) and mass concentration. The extinction efficiency is determined by particle size, refractive index and wave length. Aerosol size can grow bigger as ambient relative humidity increases, which is known as aerosol hygroscopic growth. The overall extinction coefficient of all aerosols also depends on mixing state among aerosols. Therefore, AOD is closely related a series of affecting factors from both aerosol physical properties, mass concentration and meteorological conditions.

In M1, M5, M6 and M7, particle size distribution is described by a lognormal function with a geometric mean radius and a geometric standard deviation basically based on OPAC (Optical properties of aerosols and clouds) database (Hess et al. 1998). In M3 and M4, sulfate, BC and OC are parameterized in bulk mode, and a sectional scheme is used for sea-salt and dust aerosols. M2 uses an 8 bins sectional aerosol scheme with size sections ranging from 39nm to 10μm. The refractive index of various aerosol components in the models are mainly taken from d'Almeida et al. (1991) or OPAC database. All models except M6 use a kappa (κ) parameterization (Petters and Kreidenweis, 2007), in which the aerosol hygroscopicity κ largely varies among different aerosol chemical components, such as $\kappa=0$ for black carbon, and $\kappa>0.6$ for inorganic aerosols, but the prescribed κ values could be different in the above models. M6 uses a different hygroscopic growth scheme following Kiehl and Briegleb (1993). WRF-Chem models assume internally mixing among aerosols within each mode and externally mixing between modes, M5 assumes inorganic and carbonaceous aerosols are internally mixed and externally mixed with soil dust and sea-salt. M6 uses an external mixture assumption among aerosols except for hydrophilic BC, which is internally mixed with other aerosols in a core-shell way.

We first look at the mass concentrations of different aerosol components because of their important roles in determining optical properties. The observed total inorganic aerosol concentration in Beijing on 19 January 2010 is about 130μg/m^3, with sulfate and nitrate being about 50 and 65μg/m^3, respectively (Figure 10). The models generally predict a much lower sulfate concentration except that the prediction from M5, which is close to observations, and M6, which shows overprediction. Most models predict lower nitrate concentration, in contrast to the overprediction by M2. In terms of inorganic aerosols, which have a similar optical properties, the total concentration (the sum of sulfate, nitrate and ammonium) from M2 (175μg/m^3) is higher than observation and other models, and this can explain the largest simulated AOD by M2. M6 simulates a similar level of inorganic aerosols to M2, but the simulated AOD is lower than other models, which could be due to a weak hygroscopicity or lower RH simulation (see Figure S14). For example, high RH on January 19 are captured by M2 and M6, but underpredicted by M6 (Figure S14a). Although M3 and M4 largely overpredict OC concentration, their simulated AOD are lower than M1 and M5 because their simulated inorganic aerosol concentrations are much lower and OC has a smaller (mass) extinction coefficient than inorganic aerosols. M1 predicts about three times larger BC concentration than the observations, although the mass extinction coefficient of BC is even larger than inorganic aerosols, the mass concentration and hygroscopicity of BC are much smaller and weaker than that of inorganic aerosols, leading to relatively lower AOD from M1 simulation. M5 and M7 predict a similar level of inorganic aerosol concentrations (80~90μg/m^3) and use a similar hygroscopic growth scheme, and this can help explain their consistency in the simulated AOD magnitude. In general, it appears the magnitude of inorganic aerosol concentrations and the hygroscopic growth efficiency (affected by varied RH) can account for or explain the simulated variations and

736 magnitudes of AOD in Beijing during the severe haze event, given the aerosol size distribution
737 and mixing state are alike among models.

738 Table 6 shows the statistics for AOD simulation at NCP sites and at all sites. In the NCP region,
739 R ranges from 0.36~0.74 for all the models. M2, M5 and M7 produce R around 0.7, indicating a
740 better simulation of AOD variations. M2 and M7 exhibit the best R (0.65) for all sites. It's
741 noteworthy that R values at the sites in NCP are larger than that at all sites, indicating the larger
742 reliability of model inputs (emissions and boundary conditions) and meteorological simulations.
743 In terms of magnitudes, all models tend to underpredict AOD in the whole domain, with NMB of
744 -2.7 to -71% in the NCP, and larger biases (NMB of -21~-75%) at all sites. M7 shows the smallest
745 MBE (-0.05) and NMB (-2.7%) and M2 produces the smallest RMSE. It is interesting to note that
746 the simulated AOD from the WRF-Chem models differed largely (-12 to -71%) between M1 and
747 M3 at the NCP sites, and the WRF-Chem model using finer grid size (M4) can produced slightly
748 smaller NMB compared with the same model using larger grid size (M3). However, as grid size
749 becomes finer, R and RMSE from M4 may become worse, although AOD magnitude improved.
750 The effect of grid resolution will be a topic of future paper.

751

752 ## 5 Summary

753 The MICS-Asia Phase III Topic 3 examines how current online coupled air quality models
754 perform in reproducing extreme aerosol pollution episodes in North China, and how high aerosol
755 loadings during these episodes interact with radiation and weather. Two hazy winter months,
756 namely January 2010 and January 2013, were studied by six modeling groups from China, Korea
757 and the United States. Predicted meteorological variables and air pollutants from these modeling

groups were compared against each other, and measurements as well. A new anthropogenic emission inventory was developed for this phase (Li et al., 2017), and this inventory along with biogenic, biomass burning, air and ship, and volcano emissions were provided to all modeling groups. All modelling groups were required to submit results based on the analysis methodology that documented in this paper.

Comparisons against daily meteorological variables demonstrate that all models can capture the observed near surface temperature and water vapor mixing ratio, but near surface wind speeds are overestimated by all models to varying degrees. The observed daily maximum downward shortwave radiation, particularly low values during haze days, were represented in the participating models. Comparisons with measurements of air pollutants, including SO_2, NO_x, CO, O_3, $PM_{2.5}$, and PM_{10}, from CARE-China and EANET networks showed that the main features of accumulations of air pollutants are represented in current generation of online coupled air quality models. The variations in observed AOD from CARE-China and AERONET networks were also reproduced by the participating models. Differences exist between simulated air pollutants, particularly ozone, which are probably related to different treatments of emission inventory, different meteorological and chemical parameterizations, and uncertainties in interpolations from original emission inventory to model grids might also contribute to these differences.

Manifold diversities were found in the predicted $PM_{2.5}$ chemical compositions, especially secondary inorganic aerosols and organic carbon. During winter haze events, the production from gas phase chemistry is inhibited, and whether including other aerosol formation pathways (such as aqueous phase chemistry), or how these chemistry is parametrized leads to the large difference between simulated concentrations of secondary inorganic aerosols. In addition,

781 differences in treatments of SOA also lead to large discrepancies between simulated OC
782 concentrations.

783 These results provide some directions for future model improvements, and underscore the
784 importance of accurately predicting aerosol concentration and compositions. Differences in the
785 simulated variations and magnitudes of AOD in Beijing during the severe haze event could be
786 explained by the differences in simulated inorganic aerosol concentrations and the hygroscopic
787 growth efficiency (affected by varied RH).

788 Previous studies have studied radiative forcing during haze event (Gao et al., 2017), but there are
789 large uncertainties in aerosol modeling during haze events and in estimating its interactions with
790 weather and climate. The uncertainties come from model inputs (land use data, model initial and
791 boundary conditions, etc.), physical and chemical mechanisms, and particularly
792 parameterizations of aerosol-radiation-weather interactions. Other companion papers with
793 respect to MICS-Asia Topic 3 will provide more insights into current knowledge of aerosol-
794 weather interactions under heavy pollution conditions.

795

796 **ACKNOWLEDGMENTS**

797 The authors would like to acknowledge support of this project from National Natural Science
798 Foundation of China (No. 91644217), and ground measurements from Yuesi Wang's research
799 group. The ground observation was supported by the National Natural Science Foundation of
800 China (41222033; 41375036) and the CAS Strategic Priority Research Program Grant
801 (XDA05100102, XDB05020103).

802

803

804

805

806

807

808 # Reference

809 Akimoto, H. (2003). "Global Air Quality and Pollution." Science, 302 (5651), 1716-1719.
810
811 Archer-Nicholls, S., et al. (2014). "Gaseous chemistry and aerosol mechanism developments for
812 version 3.5.1 of the online regional model, WRF-Chem." Geoscientific Model Development7(6):
813 2557-2579.
814
815 Baklanov, A., et al. (2014). "Online coupled regional meteorology chemistry models in Europe:
816 current status and prospects." Atmospheric Chemistry and Physics14(1): 317-398.
817
818 Baklanov, A., Brunner, D., Carmichael, G., Flemming, J., Freitas, S., Gauss, M., Hov, Ø.,
819 Mathur, R., Schlünzen, K.H., Seigneur, C. and Vogel, B., 2017. Key issues for seamless
820 integrated chemistry-meteorology modeling. Bulletin of the American Meteorological Society,
821 (2017).
822
823 Bey, I., et al. (2001). "Global modeling of tropospheric chemistry with assimilated meteorology:
824 Model description and evaluation." Journal of Geophysical Research: Atmospheres106(D19):
825 23073-23095.
826
827 Carmichael, G., et al. (2008). "MICS-Asia II: The model intercomparison study for Asia Phase II
828 methodology and overview of findings." Atmospheric Environment42(15): 3468-3490.
829
830 Carmichael, G. C., G.; Hayami, H.; Uno, I.; Cho, S.Y.; Engardt, M.; Kim, S.B.; Ichikawa, Y.;
831 Ikeda, Y.; Woo, J.H.; Ueda, H.; Amann, M. (2002). "The MICS-Asia study: model
832 intercomparision of long-range transport and sulfur deposition in East Asia." Atmospheric
833 Environment36: 175-199.
834

Carmichael, G. P., L.R. (1984). "An Eulerian transport/transformation/removel model for SO2 and sulfate-I. model development." Atmospheric Environment18(5): 937-951.

Carmichael, G. P., L.R.; Kitada, T. (1986). "A second generation model for regional-scale transport/chemistry/deposition." Atmospheric Environment20(1): 173-188.

Carmichael, G. R., Peters, L.R.; Saylor, R. D. (1991). "The STEM-II regional scale acid deposition and photochemical oxidant model-I. an overview of model development and applications." Atmospheric Environment25A(10): 2077-2090.

Carmichael, G. R., et al. (2008). "Predicting air quality: Improvements through advanced methods to integrate models and measurements." Journal of Computational Physics227(7): 3540-3571.

Carmichael, G. R., et al. (1998). "Tropospheric ozone production and transport in the springtime in east Asia." Journal of Geophysical Research: Atmospheres103(D9): 10649-10671.

Carmichael, G. R. C., G.; Hayami, H.; Uno, I.; Cho, S.Y.; Engardt, M.; Kim, S.B.; Ichikawa, Y.; Ikeda, Y.; Woo, J.H.; Ueda, H.; Amann, M. (2002). "The MICS-Asia study: model intercomparison of long-range transport and sulfur deposition in East Asia." Atmospheric Environment36: 175-199.

Carter, W.P., 2000a. Documentation of the SAPRC-99 chemical mechanism for VOC reactivity assessment. Contract, 92(329), pp.95-308.

Carter, W.P., 2000b. Implementation of the SAPRC-99 chemical mechanism into the models-3 framework. Report to the United States Environmental Protection Agency, January, 29.

Cheng, Y. F., Z., G.; Wei, C.; Mu, Q.; Zheng, B.; Wang, Z.; Gao, M.; Zhang, Q.; He, K.; Carmichael, G.; Poschl, U.; Su, Hang (2016). "Reactive nitrogen chemistry in aerosol water as a source of sulfate during haze events in China." Science Advances 2(e1601530).

Chin, M. G., P.; Kinne, S.; Torres, O.; Holben, B.N.; Duncan, B.N.; Martin, R.V.; Logan, J.A.; Higurashi, A.; Nakajima, T. (2002). "Tropospheric aerosol optical thickness from the GOCART Model and Comparisions with satellite and sun photometer measurements." Journal of Atmospheric Sciences(59).

Colarco, P., et al. (2010). "Online simulations of global aerosol distributions in the NASA GEOS-4 model and comparisons to satellite and ground-based aerosol optical depth." Journal of Geophysical Research115(D14).

D'Almeida, G. A., P. Koepke, and E. P. Shettle (1991), Atmospheric Aero-sols: Global Climatology and Radiative Characteristics,A.Deepak, Hampton, Va.

Emery, C. T., E.; Yarwood, G. (2001). Enhanced meteorological modeling and performance evaluation for two Texas ozone episodes.

Emmons, L. K. W., S.; Hess, P.G.; Lamarque, J-F.; Pfister G.G.; Fillmore, D.; Granier, C.; Guenther, A.; Kinnison, D.; Laeple, T.; Orlando, J.; Tie, X.; Tyndall, G.; Wiedinmyer, C.; Baughcum, S.L.; Kloster, S. (2010). "Description and evaluation of the Model for Ozone and Related chemical Tracers, version 4 (MOZART-4)." Geoscientific Model Development3: 43-67.

Fu, J. S., N. C. Hsu, Y. Gao, K. Huang, C. Li, N.-H. Lin, S.-C. Tsay (2012). Evaluating the influences of biomass burning during 2006 BASE-ASIA: A regional chemical transport modeling. Atmospheric Chemistry and Physics, 12, 3837-3855.

Gao, M., et al. (2016). "Response of winter fine particulate matter concentrations to emission and meteorology changes in North China." Atmospheric Chemistry and Physics16(18): 11837-11851.

Gao, M., et al. (2016). "Improving simulations of sulfate aerosols during winter haze over Northern China: the impacts of heterogeneous oxidation by NO2." Frontiers of Environmental Science & Engineering10(5).

Gao, M., et al. (2016). "Modeling study of the 2010 regional haze event in the North China Plain." Atmospheric Chemistry and Physics16(3): 1673-1691.

Gao, M., et al. (2015). "Health impacts and economic losses assessment of the 2013 severe haze event in Beijing area." Sci Total Environ511: 553-561.

Gao, M., et al. (2017). "Estimates of Health Impacts and Radiative Forcing in Winter Haze in eastern China through constraints of surface PM2.5 predictions." Environ Sci Technol.

Gery, M. W. W., G.Z.; Killus, J.P.; Dodge, M.C. (1989). "A photochemical kinetics mechanism for urban and regional scale computer modeling " Journal of Geophysical Research94(D10): 12925-12956.

Gong, D. Y. H., C.H. (2002). "<Gong and Ho, 2002.pdf>." Theoretical and Applied Climatology72: 1-9.

Grell, G. A., et al. (2005). "Fully coupled “online” chemistry within the WRF model." Atmospheric Environment39(37): 6957-6975.

Gutenther, A. K., T.; Harley, P.; Wiedinmyer, C.; Palmer, P.I.; Geron, C. (2006). "Estimates of global terrestrial isoprene emissions using MEGAN (Model of Emissions of Gases and Aerosols from Nature)." Atmospheric Chemistry and Physics6: 3181-3210.

Han, Zhiwei, Hiromasa Ueda, Kazuhide Matsuda, Renjian Zhang, Kimio Arao, Yutaka Kanai, Hisashi Hasome, 2004. Model study on particle size segregation and deposition during Asian dust events in March 2002, Journal of Geophysical Research, 109, D19205, doi: 10.1029/2004jd004920.

Han, Zhiwei. (2010). "Direct radiative effect of aerosols over East Asia with a Regional coupled Climate/Chemistry model." Meteorologische Zeitschrift, 19(3): 287-298.

Han Zhiwei, Jiawei Li, Xiangao Xia, Renjian Zhang, 2012. Investigation of direct radiative effects of aerosols in dust storm season over East Asia with an online coupled regional climate-chemistry-aerosol model. Atmospheric Environment, 54, 688-699.

Han Zhiwei, Jiawei Li, Weidong Guo, Zhe Xiong, Wu Zhang, 2013. A study of dust radiative feedback on dust cycle and meteorology over East Asia by a coupled regional climate-chemistry-aerosol model. Atmospheric Environment, 68, 54-63.

Han Zhiwei et al.,2016. Modeling organic aerosols over east China using a volatility basis-set approach with aging mechanism in a regional air quality model. Atmospheric Environment 124 , 186-198.

Hess, M., Koepke, P., Schuit, I., 1998. Optical properties of aerosols and clouds: the software package OPAC. Bull. Am. Meteorol. Soc. 79, 831-844.

Holben, B. N., Eck, T.F., Slutsker, I., Tanre, D., Buis, J.P., Setzer, A., Vermote, E., Reagan, J.A., Kaufman, Y.J., Nakajima, T. and Lavenu, F. (1998). "AERONET—A federated instrument network and data archive for aerosol characterization." Remote sensing of environment66(1): 1-16.

Holloway, T., et al. (2008). "MICS-Asia II: Impact of global emissions on regional air quality in Asia." Atmospheric Environment42(15): 3543-3561.

Huang, K. J. S. Fu, N. C. Hsu, Y. Gao, X. Dong, S.-C. Tsay, Y. F. Lam (2013). Impact assessment of biomass burning on air quality in Southeast and East Asia during BASE-ASIA. Atmospheric Environment, 78, 291-302.

Jacobson, M. Z., 2001: Global direct radiative forcing due to multicomponent anthropogenic and natural aerosols. J. Geophys. Res., 106, 1551–1568.

Janssens-Maenhout, G., et al. (2015). "HTAP_v2.2: a mosaic of regional and global emission grid maps for 2008 and 2010 to study hemispheric transport of air pollution." Atmospheric Chemistry and Physics15(19): 11411-11432.

Kiehl, J.T., Briegleb, B.P., 1993. The relative roles of sulfate aerosols and greenhouse gases in climate forcing. Science 260, 311-314.

Kim, S. W., et al. (2009). "NO2columns in the western United States observed from space and simulated by a regional chemistry model and their implications for NOxemissions." Journal of Geophysical Research114(D11).

Kim, Y. J. S., S.N.; Carmichael, G.R.; Riemer, N.; Stanier, C.O. (2014). "Modeled aerosol nitrate formation pathways during wintertime in the Great Lakes region of North America." Journal of Geophysical Research: Atmospheres119: 12420-12445.

Knote, C., et al. (2015). "Influence of the choice of gas-phase mechanism on predictions of key gaseous pollutants during the AQMEII phase-2 intercomparison." Atmospheric Environment115: 553-568.

Lack, D. A., et al. (2004). "Seasonal variability of secondary organic aerosol: A global modeling study." Journal of Geophysical Research: Atmospheres109(D3): n/a-n/a.

Lelieveld, J., et al. (2015). "The contribution of outdoor air pollution sources to premature mortality on a global scale." Nature525(7569): 367-371.

Li, M., et al. (2017). "MIX: a mosaic Asian anthropogenic emission inventory under the international collaboration framework of the MICS-Asia and HTAP." Atmospheric Chemistry and Physics17(2): 935-963.

Menon, S. H., J.; Nazarenko, N.; Luo, Y. (2002). "Climate Effects of Black Carbon Aerosols in China and India." Science.

Odum, J.R., Huffmann, T., Bowman, F., Collins, D., Flagan, R.C., Seinfeld, J.H., 1996. Gas/Particle partitioning and secondary organic aerosol yields. Environ. Sci. Technol. 30, 2580-2585.

Peters-Lidard, C. D., E. M. Kemp, T. Matsui, J.A. Santanello Jr., S.V. Kumar, J.P. Jacob, T. Clune, W.-K. Tao, M. Chin, A. Hou, J.L. Case, D. Kim, K.-M. Kim, W. Lau, Y. Liu, J. Shi, D. Starr, Q. Tan, Z. Tao, B.F. Zaitchik, B. Zavodsky, S.Q. Zhang, and M. Zupanski, Integrated modeling of aerosol, cloud, precipitation and land processes at satellite-resolved scales. Environmental Modeling & Software, 67, 149-159, doi:10.1016/j.envsoft.2015.01.007, 2015.

Petters, M.D., Kreidenweis, S.M., 2007. A single parameter representation of hygroscopic growth and cloud condensation nucleus activity. Atmos. Chem. Phys. 7, 1961-1971.

Ramanathan, V. C., G. (2008). "Global and regional climate changes due to black carbon." Nature Geoscience1(4): 221-227.

Schuster, G. L., et al. (2006). "Angstrom exponent and bimodal aerosol size distributions." Journal of Geophysical Research111(D7).

Seinfeld, J. H., and S. N. Pandis. (2006). Atmospheric chemistry and physics.

Shrivastava, M., et al. (2011). "Modeling organic aerosols in a megacity: comparison of simple and complex representations of the volatility basis set approach." Atmospheric Chemistry and Physics11(13): 6639-6662.

Stockwell, W. R., et al. (1997). "A new mechanism for regional atmospheric chemistry modeling." Journal of Geophysical Research: Atmospheres102(D22): 25847-25879.

Stoiber, R. E. W., S.N.; Huebert, B. (1987). "Annual contribution of sulfur dioxide to the atmosphere by volcanoes." Journal of Volcanology and Geothermal Research33: 1-8.

Streets, D. G., et al. (2003). "Biomass burning in Asia: Annual and seasonal estimates and atmospheric emissions." Global Biogeochemical Cycles17(4): n/a-n/a.

Sudo, K., et al. (2002). "CHASER: A global chemical model of the troposphere 1. Model description." Journal of Geophysical Research: Atmospheres107(D17): ACH 7-1-ACH 7-20.

Tao, Z., H. Yu, and M. Chin, Impact of transpacific aerosol on air quality over the United States: A perspective from aerosol-cloud-radiation interactions. Atmospheric Environment, 125: 48-60, doi:10.1016/j.atmosenv.2015.10.083, 2016.

Tao, Z., H. Yu, and M. Chin, The role of aerosol-cloud-radiation interactions in regional air quality – A NU-WRF study over the United States. Atmosphere, 6, 1045-1068, doi:10.3390/atmos6081045, 2015.

Tao, Z., J. A. Santanello, M. Chin, S. Zhou, Q. Tan, E. M. Kemp, and C. D. Peters-Lidard, Effect of land cover on atmospheric processes and air quality over the continental United States – A NASA Unified WRF (NU-WRF) model study. Atmospheric Chemistry & Physics, 13: 6207-6226, doi: 10.5194/acp-13-6207-2013, 2013.

Tsimpidi et al., 2010. Evaluation of the volatility basis-set approach for the simulation of organic aerosol formation in the Mexico City metropolitan area. Atmos. Chem. Phys., 10, 525–546.

Wang et al., 2016. Persistent sulfate formation from London Fog to Chinese haze. PNAS, 113(48), 13630–13635.

Wang, J., et al. (2014). "Impact of aerosol–meteorology interactions on fine particle pollution during China's severe haze episode in January 2013." Environmental Research Letters9(9): 094002.

Wang, T., et al. (2010). "Investigations on direct and indirect effect of nitrate on temperature and precipitation in China using a regional climate chemistry modeling system." Journal of Geophysical Research115.

Wang, Z. Maeda., T.; Hayashi, M.; Hsiao, L.F.; Liu, K.Y. (2001). "A nested air quality prediction modeling system for urban and regional scales: application for high-ozone episode in Taiwan." Water, Air, & Soil Pollution130(1): 391-396.

Xiao, H., et al. (1997). "Long-range transport of SOxand dust in East Asia during the PEM B Experiment." Journal of Geophysical Research: Atmospheres102(D23): 28589-28612.

1064 Xin, J., et al. (2015). "The Campaign on Atmospheric Aerosol Research Network of China:
1065 CARE-China." Bulletin of the American Meteorological Society96(7): 1137-1155.
1066
1067 Zaveri, R. A., et al. (2008). "Model for Simulating Aerosol Interactions and Chemistry
1068 (MOSAIC)." Journal of Geophysical Research113(D13).
1069
1070 Zaveri, R. A. and L. K. Peters (1999). "A new lumped structure photochemical mechanism for
1071 large-scale applications." Journal of Geophysical Research: Atmospheres104(D23): 30387-
1072 30415.
1073
1074 Zhang, Y., et al. (2010). "Simulating chemistry–aerosol–cloud–radiation–climate feedbacks over
1075 the continental U.S. using the online-coupled Weather Research Forecasting Model with
1076 chemistry (WRF/Chem)." Atmospheric Environment44(29): 3568-3582.
1077
1078 Zhang, Y. C., Y.; Sarwar, G.' Schere, K. (2012). "Impact of gas-phase mechanisms on Weather
1079 Research Forecasting Model with Chemistry (WRF/Chem) predictions: Mechanism
1080 implementation and comparative evaluation." Journal of Geophysical Research117(D01301).
1081
1082 Zheng et al., 2015. Heterogeneous chemistry: a mechanism missing in current models to explain
1083 secondary inorganic aerosol formation during the January 2013 haze episode in North China.
1084 Atmos. Chem. Phys., 15, 2031–204
1085
1086
1087
1088
1089
1090
1091
1092
1093

Atmos. Chem. Phys. Discuss., https://doi.org/10.5194/acp-2017-731
Manuscript under review for journal Atmos. Chem. Phys.
Discussion started: 5 September 2017

Atmospheric Chemistry and Physics Discussions

Table 1 Participating models in Topic 3

Models	M1: WRF-Chem1	M2: WRF-Chem2	M3: NU-WRF1	M4: NU-WRF2	M5: RIEMS-Chem	M6: RegCCMS	M7: WRF-CMAQ
Modelling Group	Pusan National University	University of Iowa	USRA/NASA	USRA/NASA	Institute of Atmospheric Physics	Nanjing University	University of Tennessee
Grid Resolution	45km	50km	45km	15km	60km	50km	45km
Vertical Layers	40 layers to 50mb	27 layers to 50mb	60 layers to 20mb	60 layers to 20mb	16 layers to 100mb	18 layers to 50mb	
Gas phase chemistry	RACM	CBMZ	RADM2	RADM2	CBM4	CBM4	SAPRC99
Aerosols	MADE	MOSAIC-8bin	GOCART	GOCART	Sulfate, nitrate, ammonium, BC, OC, SOA, 5 bins of soil dust, and 5 bins of sea salt	Sulfate, nitrate, ammonium, BC and POC	AE06
Chemical Boundary Conditions	Climatological data from NALROM	MOZART	MOZART GOCART	MOZART GOCART	GEOS-Chem	Climatological data	GEOS-Chem

Atmos. Chem. Phys. Discuss., https://doi.org/10.5194/acp-2017-731
Manuscript under review for journal Atmos. Chem. Phys.
Discussion started: 5 September 2017

Atmospheric Chemistry and Physics Discussions

Table 2 CARE-Chine network sites

ID	Site name	Characteristics	Longitude	Latitude
1	Beijing	AOD	116.37	39.97
2	Tianjin	Air quality*	117.21	39.08
3	Shijiazhuang	Air quality	114.53	38.03
4	Xianghe	Air quality	116.96	39.75
5	Xinglong	Air quality	117.58	40.39
6	Beijing Forest	AOD	115.43	39.97
7	Baoding	AOD	115.51	38.87
8	Cangzhou	AOD	116.80	38.28
9	Shenyang	AOD	123.63	41.52
10	Jiaozhou Bay	AOD	120.18	35.90

*Air quality: surface $PM_{2.5}$, PM_{10}, SO_2, NO_x, CO, O_3

Atmos. Chem. Phys. Discuss., https://doi.org/10.5194/acp-2017-731
Manuscript under review for journal Atmos. Chem. Phys.
Discussion started: 5 September 2017

Atmospheric Chemistry and Physics Discussions

Table 3 Performance Statistics of Meteorology Variables (RMSE and MBE units: degree for T2; g/kg for Q2; m/s for WS10; W/m^2 for SWDOWN)

Metrics	Models	T2	Q2	WS10	SWDOWN South	SWDOWN North
RMSE	M1	0.64	0.14	2.04	86.32	69.39
	M2	0.68	0.10	0.95	96.71	72.76
	M3	2.34	0.16	1.16	60.34	59.56
	M4	2.90	0.43	1.44	100.34	74.89
	M5	2.97	0.46	0.91	91.06	65.27
	M6	3.57	0.76	2.48	85.63	222.00
	M7	2.05	0.17	0.22	158.10	218.67
	Ensemble	1.81	0.10	1.28	81.96	62.51
MBE	M1	-0.19	0.02	2.01	66.58	59.94
	M2	-0.60	-0.01	0.91	83.88	62.38
	M3	-2.18	-0.04	1.11	36.44	47.74
	M4	-2.09	0.11	1.40	26.78	33.59
	M5	-2.73	0.43	0.74	49.06	51.00
	M6	-3.06	-0.56	2.37	-0.49	-202.26
	M7	-2.02	-0.12	0.15	145.24	159.02
	Ensemble	-1.71	-0.02	1.25	65.54	36.37
NMB (%)	M1	-0.07%	0.19%	17.58%	14.61%	13.34%
	M2	-0.21%	-0.12%	7.94%	18.41%	13.88%
	M3	-0.79%	-0.34%	9.73%	8.00%	10.63%
	M4	-0.75%	0.95%	12.26%	5.88%	7.48%
	M5	-0.98%	3.65%	6.45%	10.77%	11.35%
	M6	-1.10%	-4.77%	20.73%	-0.11%	-45.02%
	M7	-0.72%	-1.05%	1.31%	31.88%	35.39%
	Ensemble	-0.61%	-0.14%	10.98%	14.38%	8.10%

Atmos. Chem. Phys. Discuss., https://doi.org/10.5194/acp-2017-731
Manuscript under review for journal Atmos. Chem. Phys.
Discussion started: 5 September 2017

Atmospheric Chemistry and Physics Discussions

Table 4 Performance Statistics of Air Pollutants at the CARE-China sites (RMSE and MBE units: ppbv for gases and μg/m^3 for PM)

Metrics	Models	SO_2	NO_x	O_3	$PM_{2.5}$	PM_{10}		SO_2	NO_x	O_3	$PM_{2.5}$	PM_{10}
r	M1	0.76	0.60	0.46	0.85	0.76	MBE	-17.14	-5.53	-1.54	55.69	30.70
	M2	0.77	0.65	0.48	0.90	0.85		2.10	33.41	2.53	48.44	12.94
	M3	0.69	0.66	0.39	0.85	0.68		-15.89	-8.00	23.93	8.13	-19.92
	M4	0.67	0.61	0.42	0.88	0.73		-9.98	0.28	24.49	23.12	-3.23
	M5	0.72	0.73	0.39	0.91	0.84		-9.69	64.29	-5.30	1.68	-52.49
	M6	0.62	0.48	-	-	-		-27.53	-29.98	-	-	-
	M7	0.57	0.58	0.48	0.82	0.77		-25.56	7.85	-3.09	43.59	-21.00
	Ensemble	0.79	0.71	0.51	0.94	0.87		-14.81	8.90	6.84	30.11	-8.83
RMSE	M1	27.63	33.51	6.40	73.37	79.06	NMB (%)	-14.05	-5.41	7.37	63.57	18.93
	M2	21.00	66.30	8.15	72.44	80.72		12.13	69.58	39.87	54.07	6.38
	M3	29.50	36.87	24.76	47.20	78.21		-10.44	-6.26	306.33	9.67	-12.41
	M4	26.86	36.10	25.34	49.13	72.25		0.31	4.51	316.99	27.03	-1.78
	M5	32.17	87.48	7.90	45.32	81.00		6.83	127.45	-38.49	0.52	-32.94
	M6	33.95	48.62	-	-	-		-51.28	-48.59	-	-	-
	M7	34.75	35.88	6.89	64.25	70.19		-37.87	18.32	-7.78	48.92	-12.78
	Ensemble	24.10	29.12	8.86	45.25	56.65		-13.48	22.80	104.04	33.96	-5.77
MFB (%)	M1	-17.32	5.26	-5.06	64.34	21.98	MFE (%)	53.73	43.79	54.54	69.92	41.95
	M2	9.09	32.82	19.88	51.18	3.44		43.18	73.39	60.79	59.87	39.35
	M3	-12.96	4.52	113.60	32.67	-4.62		57.87	46.69	113.60	50.10	36.83
	M4	1.53	15.34	114.35	45.27	6.07		46.30	48.13	114.35	55.03	34.72
	M5	-20.24	67.25	-62.65	16.88	-35.15		63.69	72.07	80.92	48.17	45.09
	M6	-77.13	-56.89	-	-	-		84.21	69.66	-	-	-
	M7	-46.67	21.80	-19.50	57.19	-7.02		72.35	49.18	60.64	66.27	35.83
	Ensemble	-14.17	26.41	62.86	50.61	3.12		43.13	42.94	71.14	55.86	28.05

Atmos. Chem. Phys. Discuss., https://doi.org/10.5194/acp-2017-731
Manuscript under review for journal Atmos. Chem. Phys.
Discussion started: 5 September 2017

Atmospheric Chemistry and Physics Discussions

Table 5 Performance Statistics of Air Pollutants at the EANET sites (RMSE and MBE units: ppbv for gases and μg/m^3 for PM)

Metrics	Models	SO_2	NO_x	O_3	PM_{10}		SO_2	NO_x	O_3	PM_{10}
	M1	0.57	0.64	0.14	0.59		-0.68	0.68	-6.16	-21.03
	M2	0.59	0.45	0.30	0.75		-0.45	-0.39	5.50	3.12
	M3	0.50	0.55	0.26	0.51		-0.37	-0.21	3.67	3.55
	M4	0.45	0.55	0.25	0.49		-0.57	-0.61	4.28	2.96
	M5	0.58	0.54	0.01	0.03		-0.57	1.28	4.67	3.77
r	**M6**	0.33	0.24	-	-	**MBE**	0.32	-1.68	-	-
	M7	0.53	0.49	0.38	0.55		-0.03	0.64	-1.89	-15.75
	Ensemble	0.60	0.66	0.32	0.59		-0.34	-0.07	1.68	-3.89
	M1	-46.45	41.49	-15.03	-82.29		1.18	1.37	8.23	23.39
	M2	-29.64	-29.75	13.47	18.90		1.01	1.35	7.29	10.01
	M3	-25.42	-17.75	9.01	19.46		1.02	1.02	6.44	13.71
NMB	**M4**	-39.63	-35.84	10.47	16.95	**RMSE**	1.14	0.97	6.35	13.78
(%)	**M5**	-34.23	38.50	11.38	31.80		1.27	2.75	12.27	23.10
	M6	12.63	-93.57	-	-		1.38	1.85	-	-

Atmos. Chem. Phys. Discuss., https://doi.org/10.5194/acp-2017-731
Manuscript under review for journal Atmos. Chem. Phys.
Discussion started: 5 September 2017

Atmospheric Chemistry and Physics Discussions

M7	17.42	31.47	-4.71	-56.18	1.04	1.57	6.52	18.76
Ensemble	-20.76	-10.79	4.10	-8.56	0.96	0.79	4.98	11.69

Atmos. Chem. Phys. Discuss., https://doi.org/10.5194/acp-2017-731
Manuscript under review for journal Atmos. Chem. Phys.
Discussion started: 5 September 2017

Atmospheric Chemistry and Physics Discussions

Table 6 Performance Statistics of AOD

Metrics	Models	M1	M2	M3	M4	M5	M6	M7	Ensemble
R	North China	0.63	0.74	0.57	0.51	0.68	0.36	0.71	0.77
	All	0.60	0.65	0.46	0.42	0.53	0.33	0.64	0.75
MBE	North China	-0.25	-0.10	-0.09	-0.07	-0.13	-0.21	-0.05	-0.03
	All	-0.18	-0.02	-0.01	-0.01	-0.01	-0.11	0.00	-0.12
NMB (%)	North China	-71.25	-23.28	-12.63	-9.59	-28.34	-59.19	-2.70	-30.17
	All	-74.94	-30.69	-25.68	-23.64	-28.24	-55.38	-21.12	-28.91
RMSE	North China	0.35	0.20	0.26	0.28	0.24	0.36	0.22	0.22
	All	1.16	1.13	1.15	1.15	1.15	1.17	1.14	0.20

Atmos. Chem. Phys. Discuss., https://doi.org/10.5194/acp-2017-731
Manuscript under review for journal Atmos. Chem. Phys.
Discussion started: 5 September 2017

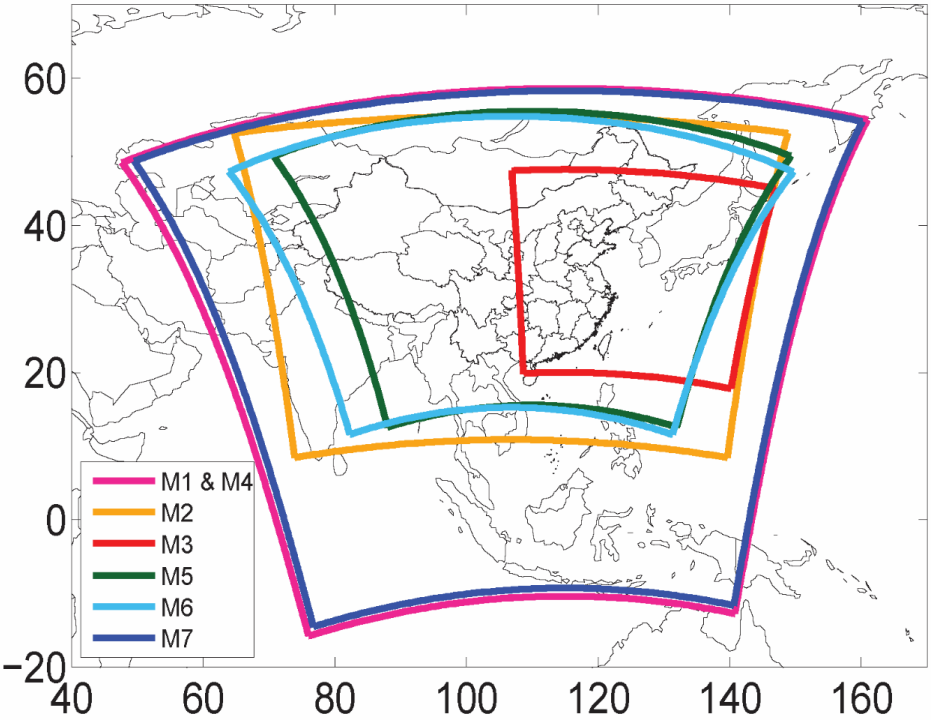

Figure 1. MICS-ASIA III Topic 3 modeling domains (descriptions of each model are documented in Table 1)

Atmos. Chem. Phys. Discuss., https://doi.org/10.5194/acp-2017-731
Manuscript under review for journal Atmos. Chem. Phys.
Discussion started: 5 September 2017

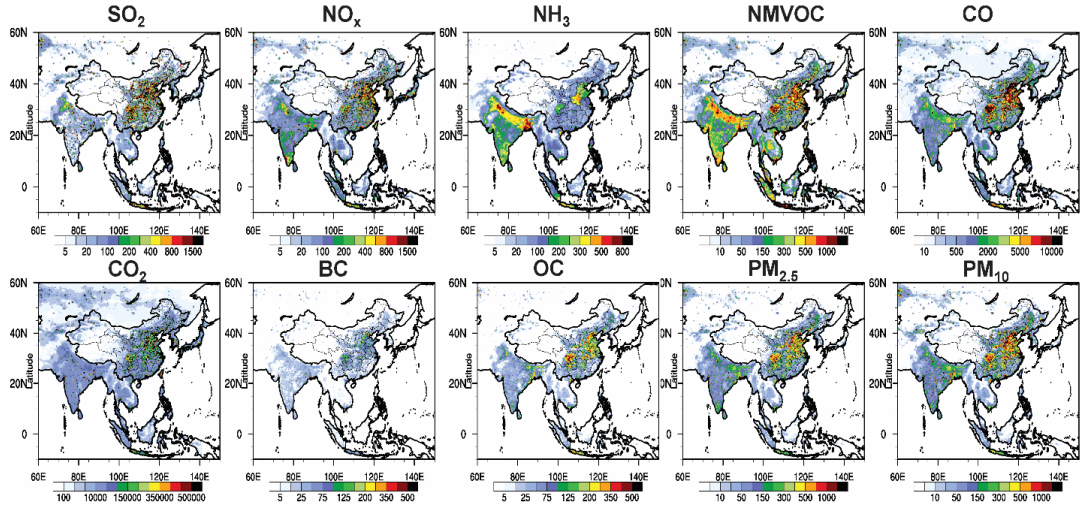

Figure 2. MIX emission inventory for January 2010 (Mg/month/grid)

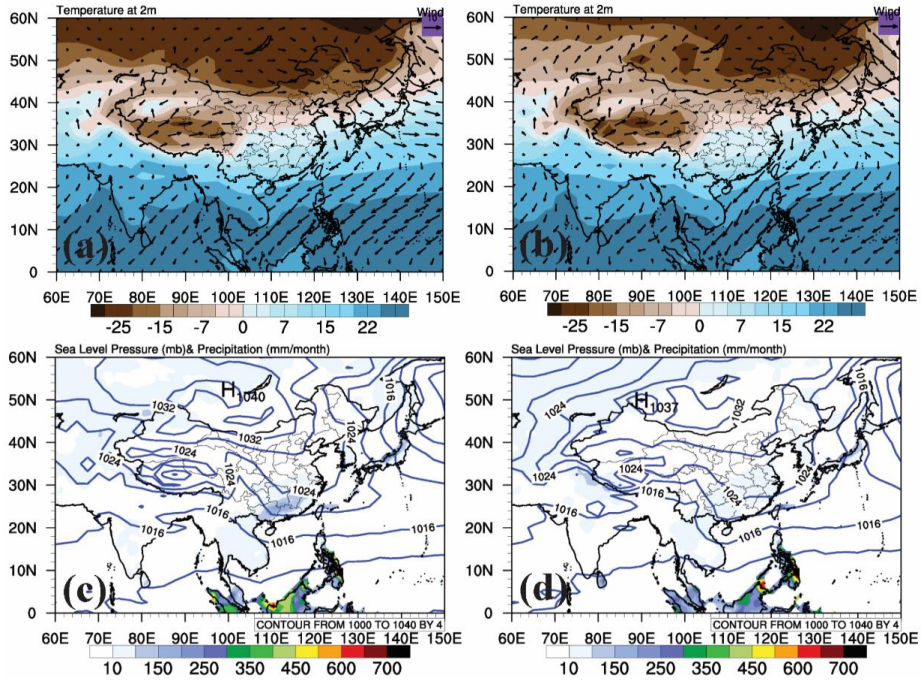

Figure 3. Monthly mean temperature at 2m, winds at 10m, total precipitation and sea level pressure for January 2010 (a,c) and January 2013 (b,d)

Atmos. Chem. Phys. Discuss., https://doi.org/10.5194/acp-2017-731
Manuscript under review for journal Atmos. Chem. Phys.
Discussion started: 5 September 2017

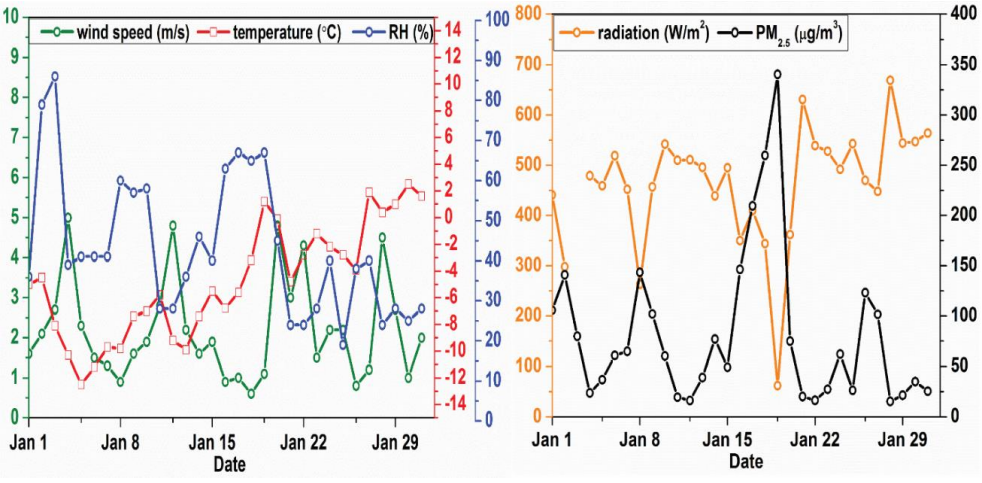

Figure 4. Observed near surface daily meteorological variables and $PM_{2.5}$ concentrations in Beijing for January 2010

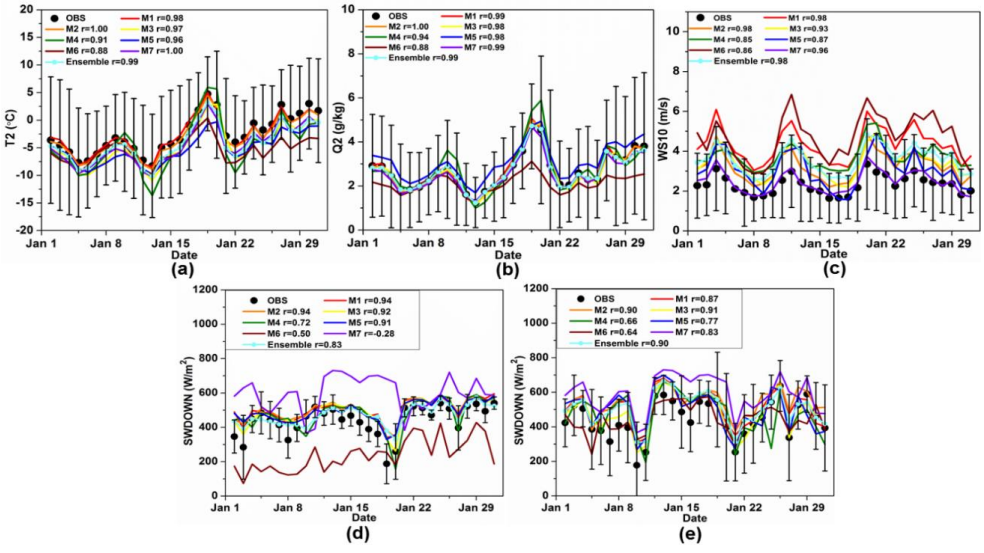

Figure 5. Comparisons between simulated and observed near surface temperature (a), water vapor mixing ratio (b), and wind speeds (c) (T2, Q2, and WS10), downward shortwave radiation in North China (d) and South China (e)

Atmos. Chem. Phys. Discuss., https://doi.org/10.5194/acp-2017-731
Manuscript under review for journal Atmos. Chem. Phys.
Discussion started: 5 September 2017

Atmospheric Chemistry and Physics Discussions

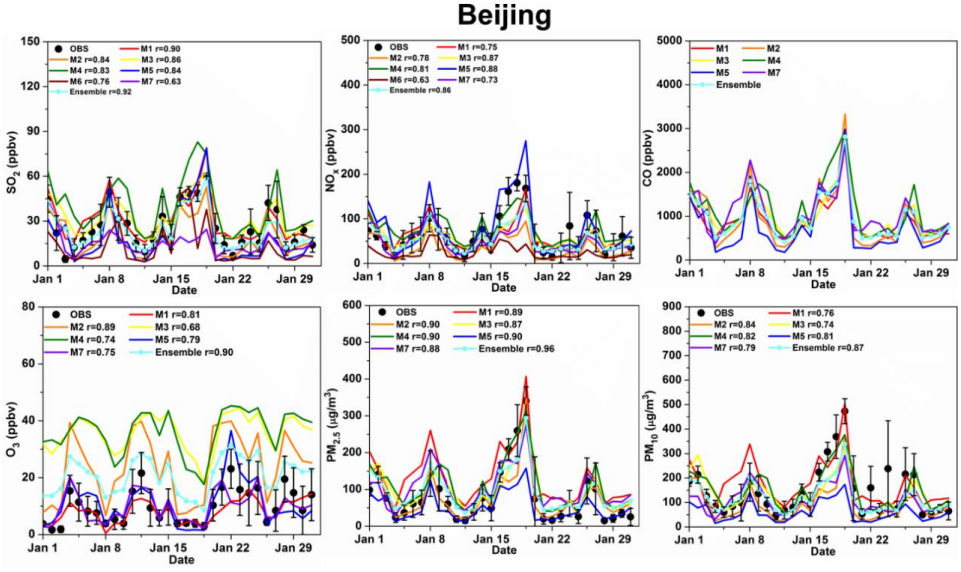

Figure 6. Comparisons between simulated and observed daily air pollutants (SO_2, NO_x, CO, O_3, $PM_{2.5}$ and PM_{10}) at the Beijing CARE-China site

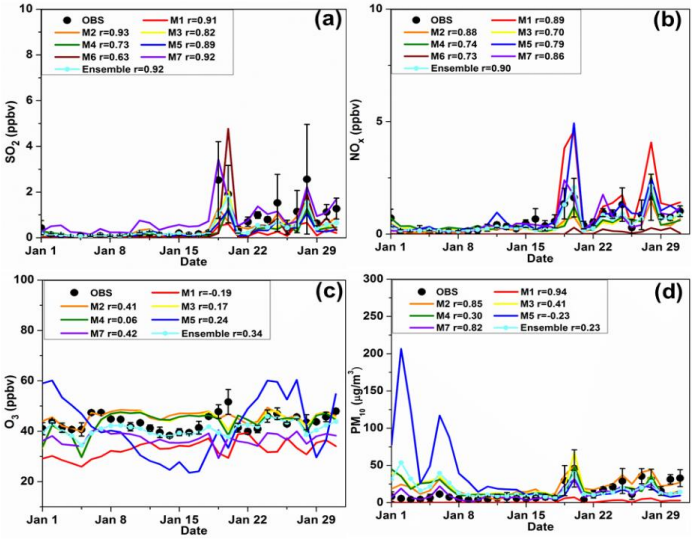

Figure 7. Comparisons between simulated and observed daily air pollutants (SO_2, NO_x, O_3, and PM_{10}) at the Rishiri EANET sites

Atmos. Chem. Phys. Discuss., https://doi.org/10.5194/acp-2017-731
Manuscript under review for journal Atmos. Chem. Phys.
Discussion started: 5 September 2017

Atmospheric Chemistry and Physics Discussions

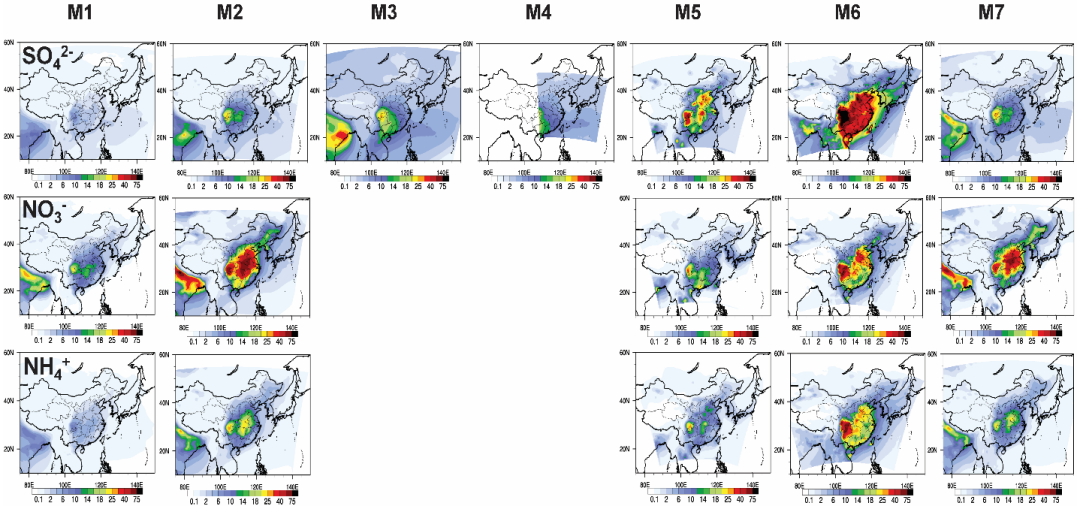

Figure 8. Simulated monthly concentrations of major $PM_{2.5}$ components ($\mu g/m^3$) for January 2010 from all participating models

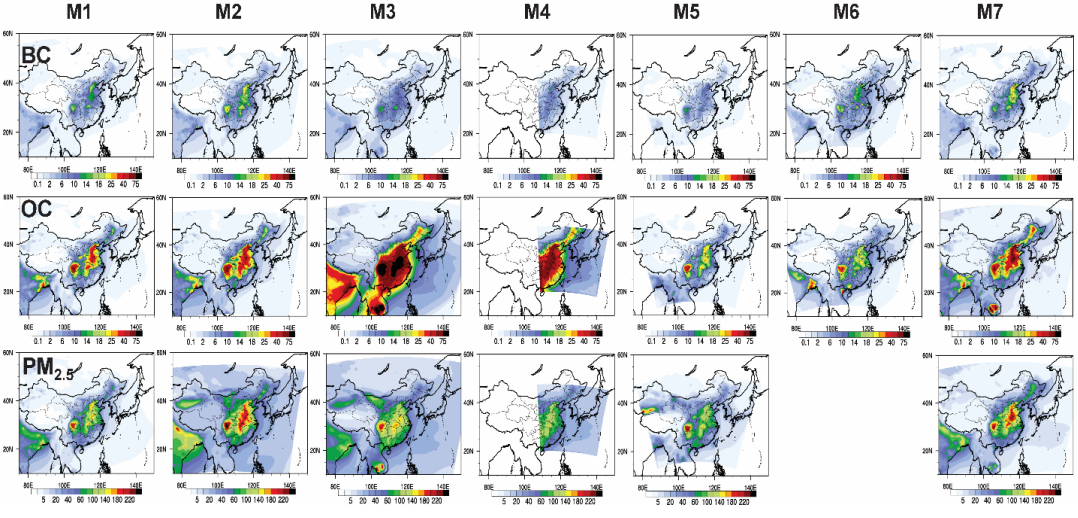

Figure 9. Simulated monthly concentrations of $PM_{2.5}$ and major $PM_{2.5}$ components ($\mu g/m^3$) for January 2010 from all participating models

Atmos. Chem. Phys. Discuss., https://doi.org/10.5194/acp-2017-731
Manuscript under review for journal Atmos. Chem. Phys.
Discussion started: 5 September 2017

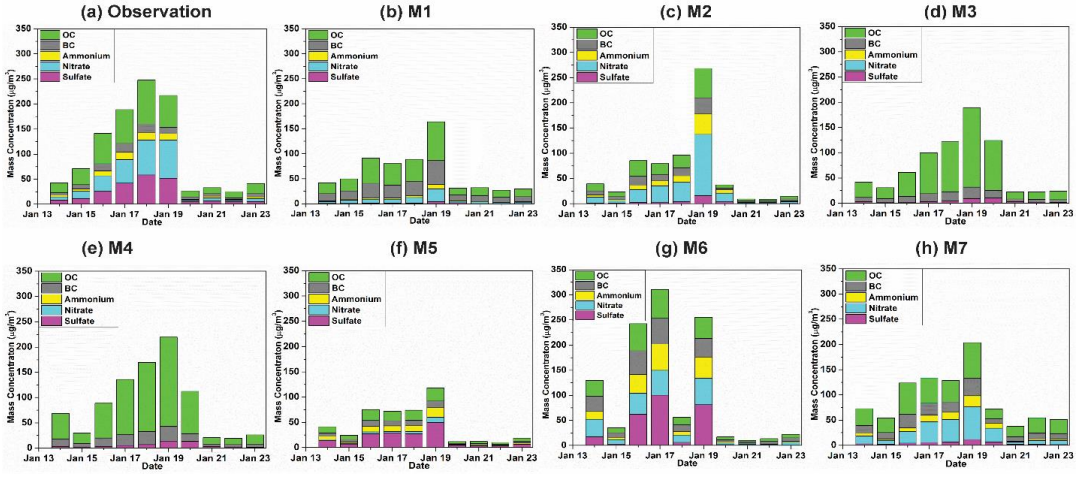

Figure 10. Observed and simulated daily mean concentrations of major $PM_{2.5}$ chemical components in the urban Beijing site

Atmos. Chem. Phys. Discuss., https://doi.org/10.5194/acp-2017-731
Manuscript under review for journal Atmos. Chem. Phys.
Discussion started: 5 September 2017

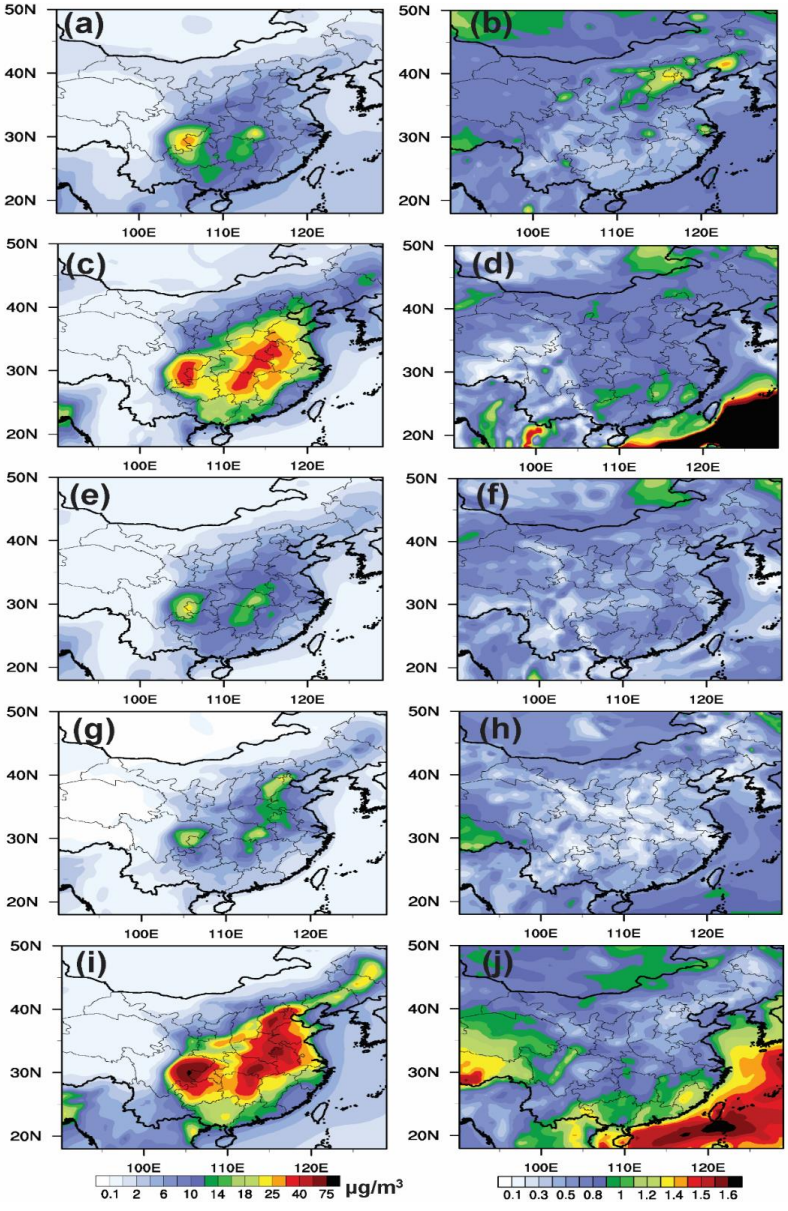

Figure 11. The ensemble mean monthly averaged near-surface distributions of $PM_{2.5}$ compositions for January 2010 (sulfate (a), nitrate (c), ammonium (e), BC (g), and OC (i)), along with the spatial distribution of the coefficient of variation ((b), (d), (f), (h), and (j), standard deviation divided by the average)

Atmos. Chem. Phys. Discuss., https://doi.org/10.5194/acp-2017-731
Manuscript under review for journal Atmos. Chem. Phys.
Discussion started: 5 September 2017

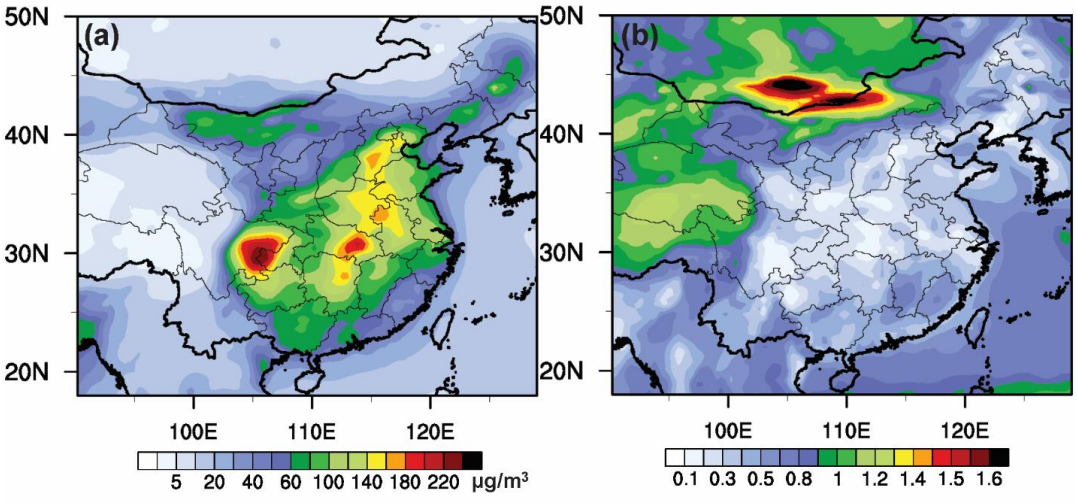

Figure 12. The ensemble mean monthly averaged near-surface distributions of $PM_{2.5}$ for January 2010 (a), along with the spatial distribution of the coefficient of variation (b, standard deviation divided by the average)

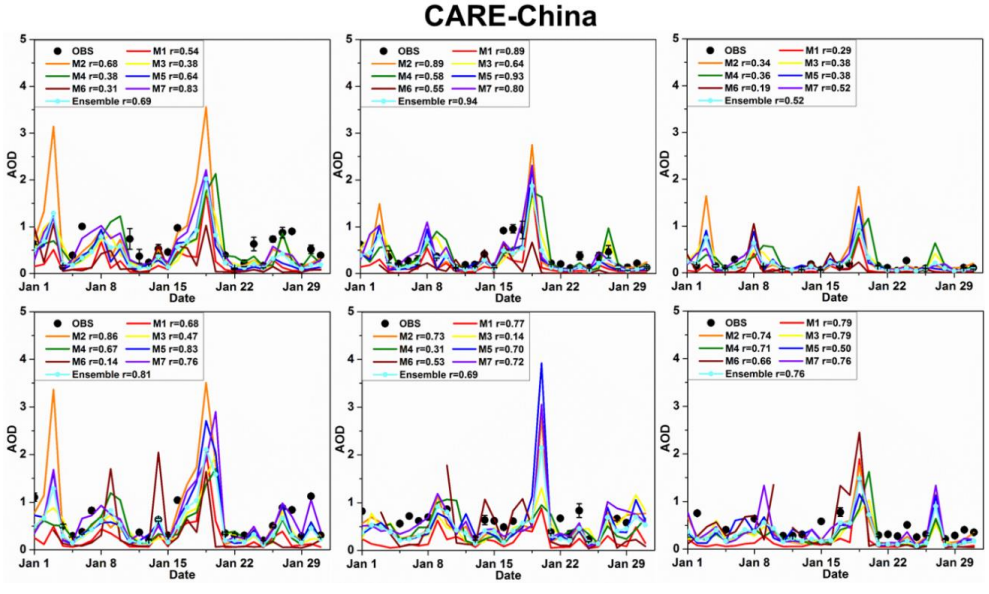

Atmos. Chem. Phys. Discuss., https://doi.org/10.5194/acp-2017-731
Manuscript under review for journal Atmos. Chem. Phys.
Discussion started: 5 September 2017

Atmospheric Chemistry and Physics Discussions

Figure 13. Comparisons between simulated and observed AOD at the CARE-China sites

(Baoding, Beijing City, Beijing Forest, Cangzhou, Jiaozhou, Shenyang,)

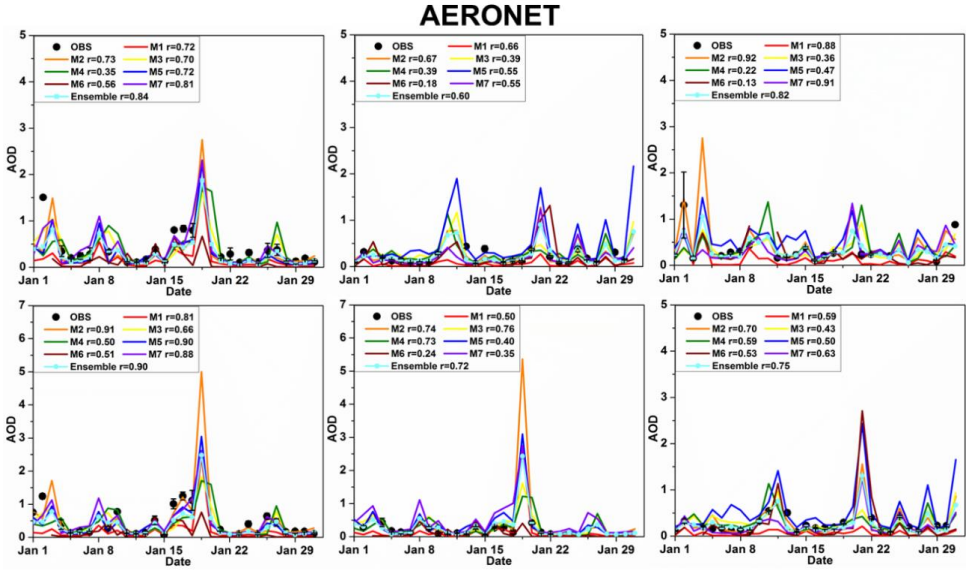

Figure 14. Comparisons between simulated and observed AOD at the AERONET sites (Beijing,

Shirahama, GIST, Xianghe, Xinglong, Osaka)